International Scientific-Technical and Production Journal

The Paton WELDING JOURNAL

December 2003 # 12

English translation of the monthly «Avtomaticheskaya Svarka» (Automatic Welding) journal published in Russian since 1948

Founders: *The E.O. Paton Electric Welding Institute of the NAS of Ukraine International Association «Welding»* **Publisher:** *International Association «Welding»*

Address:
E.O. Paton Electric Welding Institute,
International Association «Welding»,
11, Bozhenko str., 03680, Kyiv, Ukraine
Tel.: (38044) 227 67 57
Fax: (38044) 268 04 86
E-mail: journal@paton.kiev.ua
http://www.nas.gov.ua/pwj

State Registration Certificate
KV 4790 of 09.01.2001

Subscriptions:
$460, 12 issues per year,
postage and packaging included.
Back issues available.

CONTENTS

RESIDUAL STRESSES IN EXPLOSION TREATED PIPES

V.G. PETUSHKOV
E.O. Paton Electric Welding Institute, NASU, Kyiv, Ukraine

The problem of inducing circumferential compressive residual stresses in pipes has been studied. Topicality of such studies is attributable to the possibility of using their results to form the assigned fields of residual stresses and strains in pipelines in order to prevent extended fractures and relieve residual welding stresses by explosion treatment, as well as to develop a sufficiently simple procedure for estimation of its efficiency. Described is the approximation procedure for analytical estimation of stresses induced in a thin-walled pipe with a single annular explosive charge, provided that distribution of plastic strains along the generating line is close to the axially symmetric one (assumption of an instantaneous detonation of the explosive charge). Suggested also is a principle of modelling the stress fields thus induced in pipes of different dimension types.

Keywords: *explosion treatment of metal, residual stresses, stress relief, welded structure, pipeline, shock wave*

Residual stresses (RS) are the main factors that determine the load-carrying capacity and durability of welded structures operating under conditions of aggressive environments, low temperatures, cyclic loads etc. [1, 2]. Relief or redistribution of residual welding stresses, as well as inducing of the RS fields may have in many cases a decisive positive effect on operational reliability of metal structures [3]. Utilisation of a local explosion treatment of metal as a pulse process realised by using a high-density energy source and characterised by a high reproducibility of final results of the treatment may be very helpful for handling this problem [4].

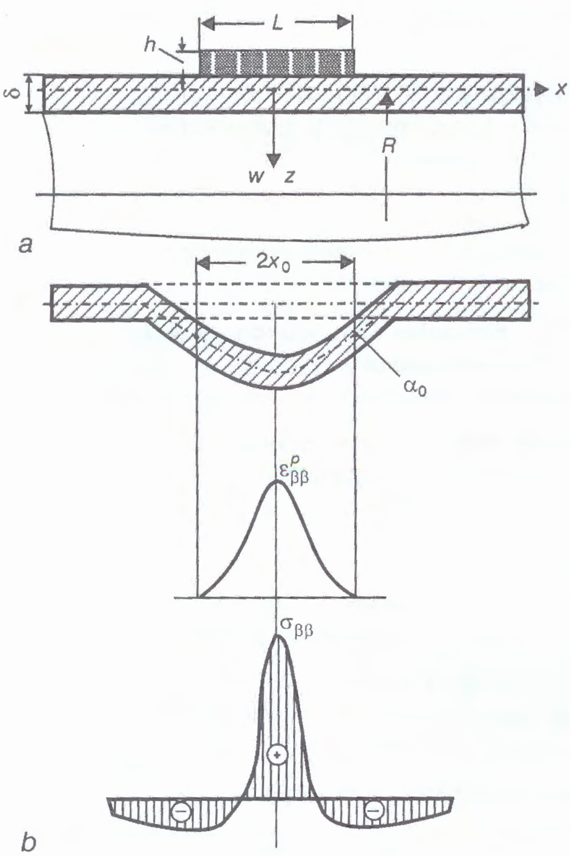

Figure 1. Flow diagram of explosion treatment of pipe (*a*) and distribution of circumferential plastic residual strains and stresses in it (*b*)

From this standpoint, of special interest is formation (by using explosion treatment) of the fields of residual stresses and strains in base metal of gas pipelines, providing retardation of initiation and development of spontaneous fracture, control of its propagation path [5], and relief of welding stresses in circumferential welds on pipes [6]. Such a problem was addressed in study [7] by an example of explosion treatment of a pipe with two annular explosive charges, each having width L and spaced at distance $b \approx L$, in an assumption that the pressure pulse has a rectangular shape, and that the circumferential plastic residual strains are constant and equal within the limits of L

$$\varepsilon_p^0 \approx \nu \frac{Q\tau_0}{R\delta\rho} - \frac{\sigma_y}{E},$$

where Q is the pressure pulse with duration τ_0; ρ is the material density; R and δ are the median radius and thickness of the pipe wall, respectively; ν is the Poisson's ratio equal approximately to 0.3; and E is the elasticity modulus. This loading allows circumferential compressive residual stresses to be formed in a zone with width b, the level of which may amount to the static yield stress σ_y at a proper selection of Q, τ_0, R and b.

This article describes an approximation procedure for analytical estimation of circumferential residual stresses induced in a thin-walled pipe with a single annular explosive charge, providing that distribution of plastic strains along the generating line is close to the actual one. Also, the principle of modelling the fields of such stresses in pipes of different dimension types is suggested.

Consider an infinite cylindrical pipe of an isotropic material with median radius R and wall thickness δ (Figure 1). A powerful annular explosive charge with width L and thickness h, located symmetrically about axis z, induces a plastic strain localised in region $2x_0$. The problem can be solved within the framework of the deformation plasticity theory.

Based on the theory of thin-walled shells [8] and according to study [9], for the case under consideration relating to axially symmetric loading, in an assumption of plastic strain components $\varepsilon^p_{\beta\beta}$ and ε^p_{xx} being constant through thickness of a pipe, write down the equation for the total residual radial displacement w of a cylindrical shell:

$$\frac{d^4w}{d\alpha^4} + 4m^4w = -4m^4R\bar{\varepsilon}^p_{\beta\beta}, \quad (1)$$

where

$$\bar{\varepsilon}^p_{\beta\beta} = \frac{1}{\delta}\int_{-\delta/2}^{+\delta/2}\varepsilon^p_{\beta\beta}dz;\ m = \sqrt{\frac{R}{\delta}}\sqrt{3(1-\nu^2)};\ \alpha = \frac{x}{R};\ \alpha_0 = \frac{x_0}{R}.$$

Assume variations of circumferential plastic strain $\varepsilon^p_{\beta\beta}$ in a direction of axis x by the following a priori relationship:

$$\varepsilon^p_{\beta\beta} = \frac{\varepsilon^0_p}{\varepsilon^4_0}(\alpha_0^2 - \alpha^2)^2\theta(\alpha_0 - |\alpha|), \quad (2)$$

where

$$\varepsilon^0_p = \varepsilon^p_{\beta\beta}\,|_{\,\alpha=\alpha_0};\ \theta(\alpha_0 - |\alpha|) = \begin{cases}1, & \alpha_0 > |\alpha|,\\ 0, & \alpha_0 < |\alpha|.\end{cases}$$

Distribution (2) is symmetric about the origin of coordinates, which satisfies conditions of gradual variations of circumferential plastic strains along axis x:

$$\varepsilon^p_{\beta\beta}\,\Big|_{\,\alpha=\alpha_0} = 0;\ \frac{d\varepsilon^p_{\beta\beta}}{d\alpha}\,\Big|_{\,\alpha=\alpha_0} = 0.$$

Solution to (1) is found separately for regions $\alpha \le \alpha_0(w_1)$ and $\alpha > \alpha_0(w_2)$, allowing for the fact that functions w_1 and w_2 are symmetric about point $x = x_0$, and that w_2 is additionally limited at $\alpha \to \pm\infty$:

$$w_1 = V_1\,\mathrm{ch}\,m\alpha\cos m\alpha + V_2\,\mathrm{sh}\,m\alpha + w_1'';$$

$$w_2 = e^{-m|\alpha|}(V_3\cos m\alpha + V_4\sin m|\alpha|_1),$$

where w_1'' is some particular solution of equation (1), which can be conveniently written down, e.g., as follows:

$$w'' = -\frac{\varepsilon^p_0R}{\alpha_0^4}\left[(\alpha^2-\alpha_0^2)^2 - \frac{6}{m^4}\right].$$

Therefore, the problem is reduced to finding four constants V_1–V_4 from a condition of join of solution at point $\alpha = \alpha_0$:

$$\frac{d^nw_1}{d\alpha^n}\,|_{\,\alpha=\alpha_0} = \frac{d^nw_2}{d\alpha^n}\,|_{\,\alpha=\alpha_0},\quad n = \overline{0.3}.$$

At $n = 0.1$ these equalities result from continuity of function w and its derivative at point $\alpha = \alpha_0$, whereas at $n = 2$ and 3 they result from continuity of intersecting forces and their moments. Then the total residual deflection and its elastic component w_y, respectively, are as follows:

$$w = -\varepsilon^0_pR\left[3F_1(m, \alpha, \alpha_0) + \frac{1}{\alpha_0^4}(\alpha_0^2-\alpha^2)^2\right]; \quad (3)$$

$$w_y = -3\varepsilon^0_pRF_1(m, \alpha, \alpha_0). \quad (4)$$

Expressions for circumferential, $\sigma_{\beta\beta}$, and axial, σ_{xx}, components of stresses in this case can be derived from the following formulae [9]:

$$\sigma_{\beta\beta} = \frac{1}{\delta}\left(N_2 - \frac{3M_2}{(\delta/2)^2}z\right);\ \sigma_{xx} = -\frac{1}{\delta}\frac{3M_1}{(\delta/2)^2}z,$$

where

$$N_2 = E\delta\left(-\frac{w}{R} - \varepsilon^p_{\beta\beta}\right);\ M_1 = -2E/3R^2\frac{(\delta/2)^2}{1-\nu^2}\frac{d^2w}{d\alpha^2},$$

$$M_2 = \nu M_2.$$

These formulae are finally reduced to the following form:

$$\sigma_{\beta\beta} = 3\varepsilon^0_pE\left[F_1(m, \alpha, \alpha_0) + \frac{2\nu z}{(1-\nu^2)R}F_2(m, \alpha, \alpha_0)\right]; \quad (5)$$

$$\sigma_{xx} = \frac{6\varepsilon^0_pEz}{(1-\nu^2)R}F_2(m, \alpha, \alpha_0). \quad (6)$$

Expressions (3) through (6) comprise the following designations:

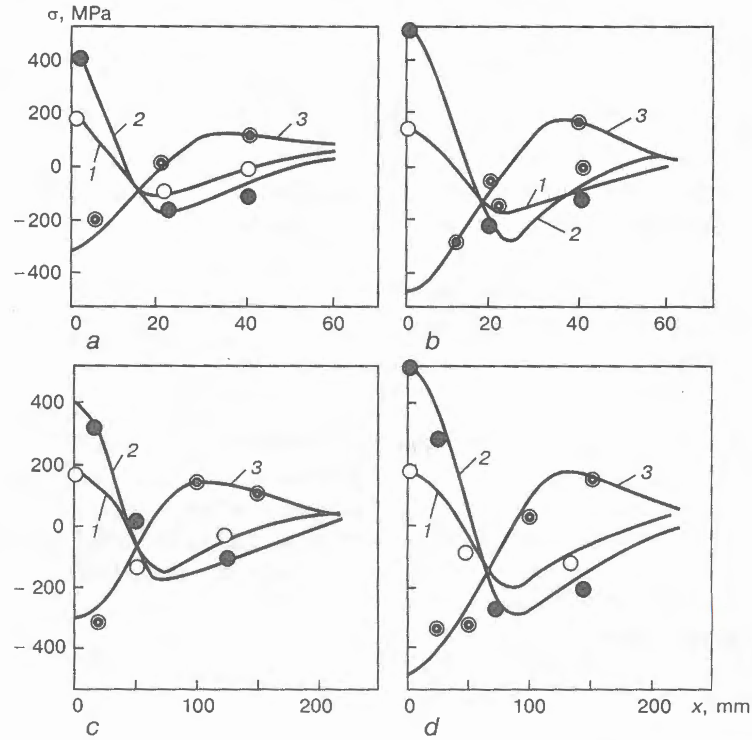

Figure 2. Calculation diagrams of circumferential (*1, 2* — external and internal surfaces, respectively) and axial (*3* — internal surface) RS induced by explosion treatment; points — experimental data (see the rest of the explanations in the text)

$$F_1(m, \alpha, \alpha_0) = \frac{1}{\alpha_0^4}\left\{e^{\xi_1}[\omega_1 \cos \xi_1 - \eta_1 \sin \xi_1] + e^{-\xi_2}\left[\omega_1 \cos \xi_2 - \eta_1 \sin \xi_2 - \frac{2}{m}\right]\right\} \times$$

$$\times\, \theta(\alpha_0 - |\alpha|) + \frac{1}{\alpha_0^4 m^3}\left\{e^{\xi_2}[\omega_1 \cos \xi_2 - \eta_1 \sin \xi_2] + e^{-\xi_1}\left[\omega_2 \cos \xi_1 - \eta_2 \sin \xi_1 - \frac{2}{m}\right]\right\}\theta(|\alpha| - \alpha_0);$$

$$F_2(m, \alpha, \alpha_0) = \frac{1}{\alpha_0^4 m}\left\{e^{-\xi_2}[\omega_1 \sin \xi_2 - \eta_1 \cos \xi_2] - e^{-\xi_1}[\omega_1 \sin \xi_1 + \eta_1 \cos \xi_1] + 2\left(\alpha^2 - \frac{1}{3}\alpha_0^2\right)\theta(\alpha_0 - |\alpha|)\right\} +$$

$$+ \frac{1}{\alpha_0^4 m^3}\left\{e^{\xi_2}[\omega_1 \sin \xi_2 - \eta_1 \cos \xi_2] + e^{-\xi_1}[\omega_2 \sin \xi_1 - \eta_2 \cos \xi_1]\right\}\theta(|\alpha| - \alpha_0);$$

$$\xi_1 = m(|\alpha| - \alpha_0); \quad \xi_2 = m(|\alpha| + \alpha_0);$$

$$\eta_1 = \alpha_0 + \frac{2}{3}\alpha_0^2 m; \quad \eta_2 = \alpha_0 - \frac{2}{3}\alpha_0^2 m.$$

At $z = \pm 0.5\delta$, expressions (5) and (6) are used to determine components of stresses on the internal and external surfaces of a pipe:

$$\sigma_{\beta\beta}\Big|_{z = \pm 0.5\delta} = 3\varepsilon_p^0 E\left[F_1(m, \alpha, \alpha_0) \pm \frac{\nu\delta}{(1 - \nu^2)R} F_2(m, \alpha, \alpha_0)\right]; \quad (7)$$

Characteristics of stress-strain states of explosion treated pipes

Treatment mode	*Pipe parameters, mm*		*Characteristics*						
			Explosive charge		*Stress-strain state*				
	R	*δ*	$\rho_0 h$, *g/cm²*	*L/δ*	ε_p^0, %	$\varepsilon_p^0/\varepsilon_y$	α_0	x_0, *mm*	σ_{max}
Figure 2, *a*	105	5	0.099	1.68	0.29	1.59	0.184	19.3	290
Figure 2, *b*	105	5	0.097	2.39	0.43	2.33	0.236	24.8	330
Figure 2, *c*	503	14	0.255	1.68	0.29	1.59	0.139	71.6	290
Figure 2, *d*	503	14	0.251	2.39	0.43	2.33	0.178	91.7	330

$$\sigma_{xx}\Big|_{z=\pm0.5\delta} = \pm\frac{3\varepsilon_p^0 E\delta}{(1-\nu^2)R} F_2(m, \alpha, \alpha_0). \qquad (8)$$

Parameter α_0 is determined from a condition of similarity of experimental diagrams of RS and those calculated from formulae (7) and (8), and ε_p^0 — from a condition of equality of maximal values of these stresses in surface layers of the pipe. Note that analysis of experimental data given in [10] proves a satisfactory coincidence of the level and character of distribution of actual welding residual stresses with those assigned by formulae (7) and (8). This is indicative of the fact that the local explosion treatment can simulate welding stresses, ensuring high reproducibility of stress diagrams.

Demonstrate now how results of explosion treatment of one pipe can be applied to a pipe of a different diameter without the use of any extra experiments. To do this, consider by a specific example the problem of modelling of parameters of an explosive charge required for inducing similar distributions (diagrams) of RS in pipes with different geometric characteristics. The pipe used as a reference, which is convenient for experimental studies, was that with R = 105 mm and δ = 5 mm, made from steel 17G1SU. Explosion treatment was performed by the flow diagram shown in Figure 1. The values of ε_p^0 and α_0 (Table) providing closeness of the theoretical curves of distribution of stresses plotted by using expressions (7) and (8) to the measurements were selected from the experimental diagrams of RS (plotted on the basis of tensometry by cutting the pipe into rings). These curves are shown in Figure 2, *a* and *b*, for two different conditions of loading the pipes (*a* — for pipe ∅ 210×5 mm at $\rho_0 h$ = = 0.099 g/cm^2 and L/δ = 1.68; *b* — same at $\rho_0 h$ = = 0.097 g/cm^2 and L/δ = 2.39). Maximal values of residual stresses, including those close in level to σ_y, are achieved at point α_0.

The value of the rest of the stress components can be determined from formulae (7) and (8), providing that $\sigma_{\beta\beta}^{+0.5\delta}$, $\sigma_{\beta\beta}^{-0.5\delta}$, $\sigma_{xx}^{+0.5\delta}$ or any of their combinations are assigned.

Equality of a maximal value of $\frac{1}{2}\left(\sigma_{\beta\beta}^{+0.5\delta} + \sigma_{\beta\beta}^{-0.5\delta}\right)$ designated as σ_{max} was used for convenience as the basis of modelling, in addition to constancy of ε_p^0. Theoretical diagrams of RS for a pipe (call it the model one) with R = 503 mm and δ = 14 mm, made from the same steel, are shown in Figure 2, *c* and *d* (*c* — at $\rho_0 h$ = 0.255 g/cm^2 and L/δ = 1.68; *d* — at $\rho_0 h$ = 0.251 g/cm^2 and L/δ = 2.39). The value of α_0 is estimated automatically from the values of ε_p^0 and σ_{max} (see the Table).

Diagrams of total residual displacements w and corresponding elastic components w_y (Figure 3), coinciding in a region with zero plastic circumferential strains, were also calculated from formulae (3) and (4). Convergence of the data of direct measurements of the total and elastic components of residual deflections (points in Figure 3) with the calculated curves is indicative of the coincidence of theoretical and experimental values of residual stresses within the framework of the found solution of equation (1), which is proved by the data shown in Figure 3.

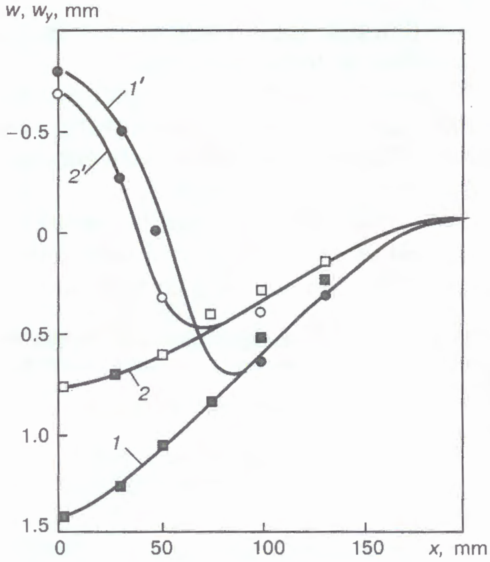

Figure 3. Distribution of radial displacements along the generating line of pipe with $R\times\delta$ = 503×14 mm (*1* — w, *2* — w_y for the internal surface; *1'*, *2'* — for the external surface); points — experimental data

Selection of the explosion treatment parameters that ensure corresponding stressed states in model and reference pipes can be done in the first approximation in accordance with the dimensional theory, allowing for the energy balance of an explosive. The explosion treatment processes will be similar, provided that, e.g., the value of L/δ and energy parameter $(\rho_0 h/\delta)\sqrt{Q/\sigma_y}$, allowing for the dependence of the explosion loading conditions upon the pipe material strength, remain constant. In this case the σ_{max} equality condition for the model and reference pipes should be replaced by the condition of equality of relationships $\sigma_{max}^{m}/\sigma_{max}^{r} = \sigma_y^m/\sigma_y^r$.

Also, it should be noted that theoretical dependencies used to calculate the explosive parameters from the strength and geometry characteristics of a pipe and the required values of parameters ε_p^0 and α_0, determining the RS field induced by explosion, can be derived by way of a separate analysis of the process of local explosion treatment.

CONCLUSIONS

1. It was proved that explosion treatment could induce in thin-walled pipes the RS fields similar to those formed during circumferential arc welding.

2. The level and character of distribution of RS induced in pipes by local explosion treatment depend upon the highest circumferential plastic strain ε_p^0, relative width α_0 of the plastic strain zone and static yield stress.

3. Residual radial displacements of a pipe, which can be readily estimated by an experimental way, can serve as the similarity criterion of residual stress-strain

states formed in thin-walled pipes of different dimension types after explosion treatment.

4. The method of scale modelling can be employed to calculate parameters of explosive charges required to induce the RS fields in pipes of different dimension types by local explosion treatment.

5. The method developed can be useful to solve some practical problems associated with relief or induction of RS in thin-walled pipe structures.

1. (1977) *Fracture*. Vol. 4. Investigation of fracture for engineering calculations. Ed. by G. Libovits. Moscow: Mashinostroenie.
2. (1981) *Fracture mechanics: Rapid fracture, crack arresting*. Moscow: Mir.
3. Holl, W.J., Kihara, H., Zoot, W. et al. (1974) *Brittle fractures of welded structures*. Moscow: Mashinostroenie.
4. Mogilyov, V.A., Ivanov, A.G., Fateev, Yu.A. (1981) Reaction of thin-walled pipes to internal explosion loading. *Fizika Goreniya i Vzryva*, **3**, 143–146.
5. Zajtsev, K.I., Anuchkin, N.P. (1973) Role of strain fields in spontaneous propagation of crack along a pipeline. *Stroitelstvo Truboprovodov*, **7**, 5–7.
6. Makhnenko, V.I., Kudinov, V.M., Petushkov, V.G. et al. (1975) Calculation of the efficiency of decreasing RS in circumferential welds on pipelines by explosion treatment. *Avtomatich. Svarka*, **12**, 6–8.
7. Makhnenko, V.I., Petushkov, V.G., Egorova, L.A. et al. (1980) Formation of circular zones with residual circumferential compressive stresses in steel pipes. *Ibid.*, **2**, 9–11.
8. Novozhilov, V.V. (1962) *Theory of thin shells*. Leningrad: Sudpromgiz.
9. Podstrigach, Ya.S., Osadchuk, V.L. (1968) On evaluation of the stressed state of thin shells allowing for the strains caused by physical-chemical processes. *Fiz.-Khim. Mekhanika Materialov*, **2**, 218–224.
10. Zhdanov, I.M., Batyuk, V.V., Kudinov, V.M. et al. (1979) Residual stresses in circumferential welds on explosion treated pipes. *Avtomatich. Svarka*, **7**, 14–16.

SPECIFICS OF FORMATION OF STRUCTURE OF JOINTS, MADE FROM DISPERSION-STRENGTHENED COMPOSITE Al + 4 % C, IN DIFFUSION BONDING

V.R. RYABOV, A.N. MURAVEJNIK, G.K. KHARCHENKO and **Yu.V. FALCHENKO**
E.O. Paton Electric Welding Institute, NASU, Kyiv, Ukraine

It is shown that the quality joints of CM 1013 and 1501 with 4 % C can be obtained in using an aluminium ductile interlayer. Optimum conditions of diffusion bonding in vacuum are given. Strength of joints of CM 1501 + 4 % C reaches 443.8 MPa, while that of CM 1013 + 4 % C joints is 295 MPa.

Keywords: *diffusion bonding, dispersion-strengthened composite, weldability, aluminium interlayer, thermodeformational cycling, structure, strength, hardness*

The dispersion-strengthened composite materials (DSCM) produced from powders using the method of mechanical alloying are used as structural materials, capable to have a stable operation under the conditions of increased temperatures and long-acting stresses, in friction units, etc. Effect of the dispersion strengthening is attained by artificially introduced ultra-dispersed (0.10–0.05 μm) insoluble particles of carbides, oxides, intermetallics, distributed uniformly in the base metal. Owing to their presence the structure, forming at deformation heat treatment, is stabilized, and high hardness, strength, wear resistance and thermal stability of the material are provided.

Among DSCM on the aluminium base, the carboaluminium, in particular composite Al + 4 % C, possesses the optimum complex of characteristics. It is produced by the method of a reaction mixing of aluminium powder with a finely-refined carbon black. The technological process includes the preparation of charge, its treatment in an attritor and manufacture of hot-pressed semi-products (rods, shapes and so on). At the final stage of the process the composite represents an aluminium matrix with ultra-dispersed inclusions of aluminium carbide Al_4C_3, uniformly distributed in it. This composite has a strength of 500 MPa order and 4–7 % elongation at room temperature. The creep strength (100 h at 350 °C) is 120 MPa [1], however, the application of these materials in structures of advanced engineering depends greatly on the capability of their welding.

The diffusion bonding was excellent in welding metallic composite materials (MCM) on the aluminium base [2–5]. The process occurs as a result of heating and plastic deformation of near-contact volumes of metals being joined without their melting, that preserves the composition of components included into MCM, their volume share and dispersity.

In this work the weldability in a free state was investigated using the method of diffusion bonding in vacuum of DSCM on the base of pure aluminium (CM 1013 + 4 % C) and Al–Mg alloy (CM 1501 + + 4 % C). Chemical composition of composites is given in Table 1.

Diffusion bonding of specimens was made in the P-155 type installation with a radiation heating and pneumohydraulic mechanism of upset force transmission. Plate-type molybdenum heaters served as sources for heating parts being joined. Specimens of composites of 32 mm diameter and 23 mm height were butt joined at 560–600 °C, upset force was 9–15 MPa, time of bonding — 10–15 mm. Chamber was evacuated to $1.33 \cdot 10^{-3}$ Pa, upsetting of specimens after bonding was not more than 10 % of initial height.

Microstructural examinations were made by the methods of optical microscopy, scanning and transmission microdiffraction electron microscopy. Determination of element composition was made in X-ray microanalyzer «Camebax», the measurement of hardness of specimens — in instrument «Rockwell» at load F = 600 N (ball), microhardness — instrument PMT-3 at F = 0.2 N.

Structure of CM, being joined, in initial (after hot pressing) state is given in Figures 1, *a* and 2, *a*.

Metallographic examinations of structure of composite 1013 + 4 % C revealed the typical dispersity of structural and phase constituents and homogeneity of their distribution in matrix metal (Figure 1, *a*). As the electron microscopic examinations showed, the precipitations of strengthening phase of 0.02–0.13 μm size have mainly the acicular nature and arranged along the boundaries and grain body. Interparticle distance is on average 0.1–1.0 μm. It was established by the microdiffraction analysis that the composition of phase formations corresponds mainly to Al_4C_3. Reflections, typical of pure carbon, are absent that proves almost complete interaction of carbon with matrix aluminium in the process of composite manufacture [6]. Particles of oxides of larger sizes (2–3 μm) are also revealed, whose morphology and distribution have a directed line nature. A fine-grain structure is characteristic of the aluminium matrix. Sizes of structural elements are 0.2–0.5 μm.

The peculiarity of a fine structure of metal of composite 1013 + 4 % C is a high volume density of dislocations ρ ($9.5 \cdot 10^{10}$–$1 \cdot 10^{11}$ cm^{-2} and higher), and also formation of non-closed loop-shaped extinction contours, characterizing the high degree of a local bending of metal lattice [6]. The latter proves the formation of structures with a high level of stresses in the composite examined. Its as-initial hardness is *HRB* 106–108.

Metallographic examinations of CM 1501 + 4 % C showed that in initial state the structure of composite

Table 1. Chemical composition of composite materials

Alloy	Mass share of elements, %					
	Cu	Mg	Si	Fe	C	Al
1013 + 4 % C	0.05	0.05	0.3	0.30	4.0	99.3
1501 + 4 % C	0.01	4.60	0.1	0.05	4.0	Res.

is not homogeneous (Figure 2, *a*). Ultra-dispersed acicular precipitations of phase Al_4C_3 are distributed quite uniformly in a light-grey matrix of composite (Figure 3) and have the same sizes as composite 1013 + 4 % C. In addition, the larger intermetallic inclusions with magnesium, which inherent in a matrix aluminium alloy (Al_3Mg_2, Mg_2Si), are observed. There are also oxide inclusions of 1–5 μm size. Microhardness of light-grey matrix of composite at 20 g load is 1500–1600 MPa. In structure of CM 1501 + 4 % C the dark-grey line formations of different sizes with an increased carbon content are also revealed (Figure 4). When scanning by an electron probe, the concentration of carbon in dark-grey regions of the parent metal 4–5 times increases its content in a light-grey matrix (see Figure 4). Microhardness of these regions is much lower as compared with that of the light-grey matrix and equals 1100–1300 MPa. These are, probably, regions, where the incomplete transformation of carbon into aluminium carbide Al_4C_3 is occurred in the process of the composite manufacture. In addition, light areas of pure aluminium with a low hardness 460–500 MPa, where the carbon concentration is reduced almost to zero, are observed. Rockwell hardness of CM 1501 + 4 % C in initial state is *HRB* 110–111.

The presence of a thermodynamically stable dense oxide film at the surface of DSCM hinders the process of bonding, therefore, the preparation of surface of specimens influences greatly the quality of joints.

In diffusion bonding of DSCM the best results were obtained when a surface layer of 0.5 mm thickness was removed by a file with a subsequent cleaning of contacting surface by a scraper directly before bonding. In this case the oxide film, available at the surface, is removed, and a film, formed anew, has a much smaller thickness that simplifies its destroying in the process of diffusion bonding and, thus, promotes the formation of the quality joint.

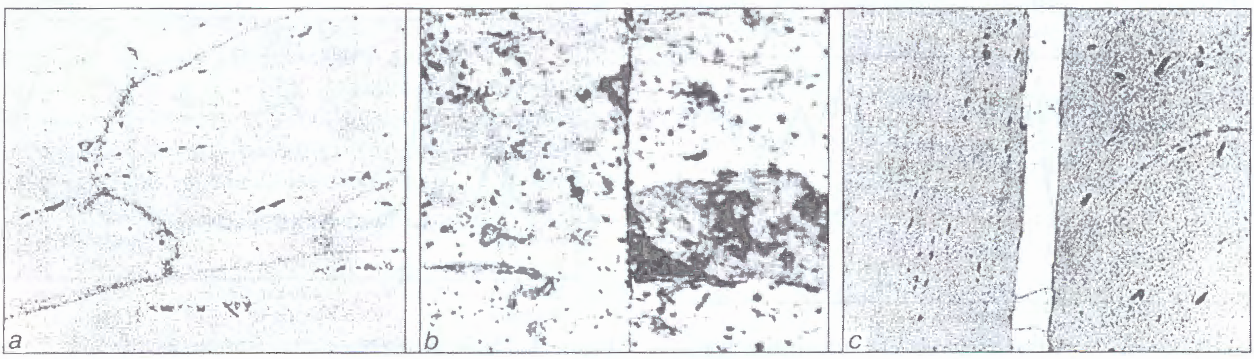

Figure 1. Structure of parent metal CM 1013 + 4 % C (*a*) and joints without (*b*) and with interlayer (*c*) from alloy AD1 (×300)

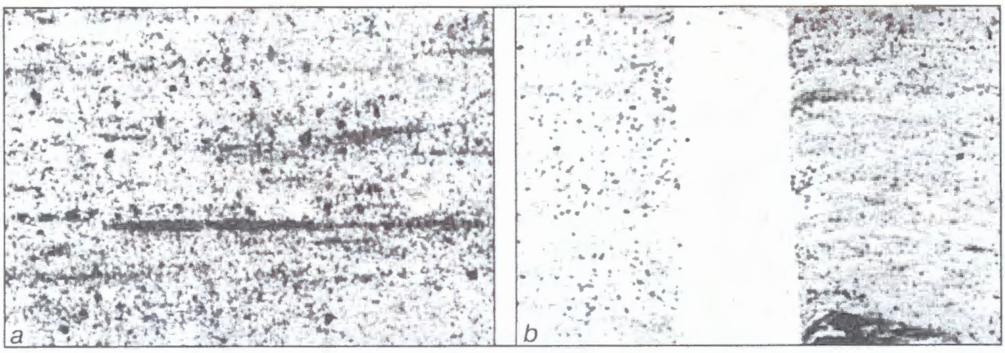

Figure 2. Structure of parent metal CM 1501 + 4 % C (*a*) and joint (*b*) with interlayer from alloy AD1 (×150)

The DSCM specimens were joined with an interlayer from aluminium alloy AD1 and without it.

At direct bonding of DSCM the quality joints are not produced. The latter are fractured at tensile tests in bond at loading of only 40 MPa. Metallographic examinations of joints of CM 1013 + 4 % C showed that the thermodeformational cycle of bonding does not almost change the composite structure. At the interface, the pores, oxides, long cracks are observed (see Figure 1, *b*). It was established by electron microscopic examinations that the formation of joints is occurred at the depth of only 0.5 μm from the both sides from the interface. From the results of the quantitative analysis, the common grains amount to not more than 1.5 % of interface, i.e. the material is so hard that the hot deformation is localized in the narrow zone, the recrystallization is difficult and the processes of volume interaction are not developed.

Thus, in direct bonding of DSCM some problems are occurred due to structure peculiarities connected with a need to provide a sufficient ductility of the material in the region of a contact interaction of materials being joined. It is known [7] that the stage of a physical contact formation is one of the most important in diffusion for the formation of the quality joint. Its formation is realized by a plastic deformation of near-contact volumes of materials being joined, while in bonding of hard-to-deform materials it is realized by deformation of a ductile interlayer (for example, from aluminium, copper nickel and others).

Bonding of CM 1013 + 4 % C was realized using a ductile interlayer from aluminium alloy AD1 of 0.015 mm thickness at temperature 600 °C, upset pressure of 9–10 MPa and 15 min time.

During metallographic examination of joints a solid interlayer from aluminium of 12–14 μm thickness is observed at the interface (see Figure 1, *c*). At separate regions the micropores and long oxide inclusions, large pores, discontinuities were not observed. Electron microscopic examinations showed that the use of interlayer of pure aluminium in bonding changes the structural state of the contact zone. A partial dissolution of strengthening phase precipitations and decrease in density of defects of the crystalline lattice $\rho \approx 10^9$ cm^{-2} is outlined, associated with the diffusion at concentration equalizing, that improves the ductility of contact surfaces and activates the formation of the joint. Mechanical tensile tests showed that the strength of joints of CM 1013 + 4 % C reaches 295 MPa, that amounts to 60 % of the parent metal strength (Table 2).

The diffusion bonding of CM 1501 + 4 % C was also performed with an interlayer from aluminium alloy AD1. Interlayers of 0.15, 0.30 and 0.45 mm thickness were used. The composite and foil surfaces being joined were cleaned by a scraper. Microstructure is presented in Figure 5 and proves a good quality of joints made with an interlayer of different thickness. Large pores, lack of fusion at the interface with an interlayer were not revealed.

Optical examinations of the microstructure of joints showed that in the variants examined the structure of the composite is not almost changed under the action of bonding temperatures and deformations. A solid interlayer of aluminium of 130 μm thickness at aluminium alloy AD1 thickness δ = 0.15 mm before bonding, 240–260 μm at δ = 0.3 mm and 330–360 μm at δ = 0.45 mm is observed at the interface. The application of thermodeformational cycling of the first variant allowed the joints to be produced at a thickness of interlayer of 90 μm (see Figure 2, *b*). In

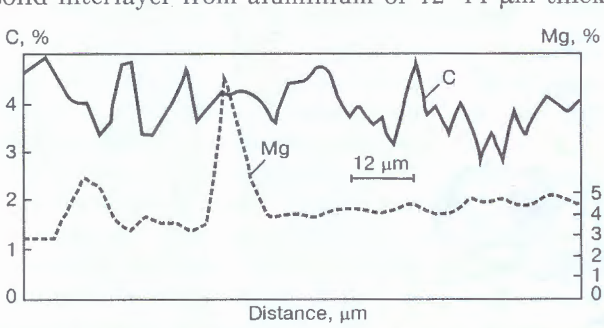

Figure 3. Nature of carbon and magnesium distribution in light-grey matrix of CM 1501 + 4 % C

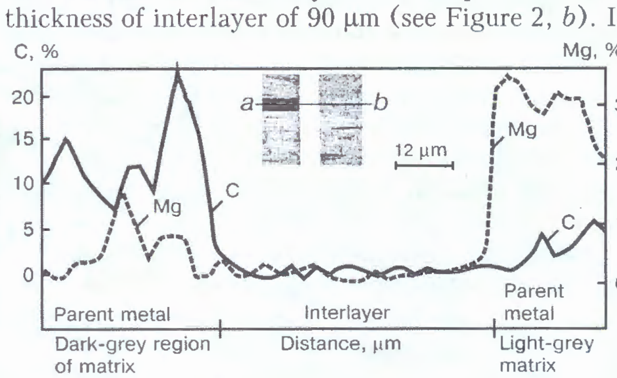

Figure 4. Nature of distribution of elements in the direction of scanning *a*–*b* in joint of CM 1501 + 4 % C in diffusion bonding

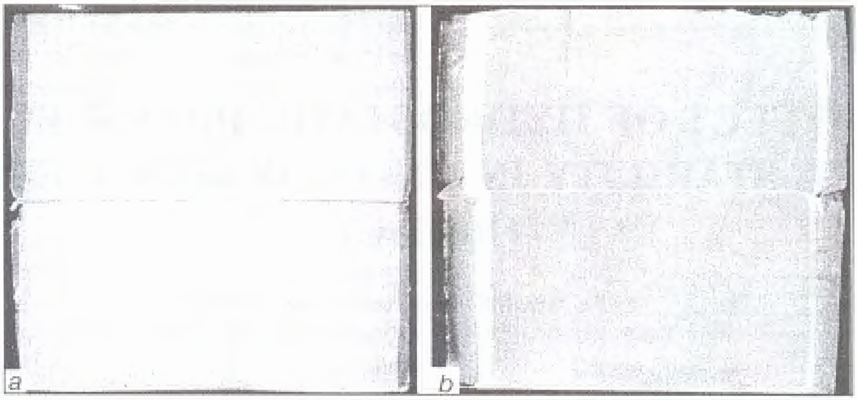

Figure 5. Macrostructure of joints of CM 1501 + 4 % C with interlayer of 0.15 (*a*) and 0.45 (*b*) mm thickness

Table 2. Conditions of diffusion bonding and properties of DSCM joints

No. of specimen	*Alloy*	*Thickness of interlayer from AD1, mm*	*T, °C*	*P, MPa*	*τ, min*	σ_t, *MPa*	*Mean value* σ_t, *MPa*
1	1013 + 4 % C	0.015	600	9–10	15	314.0–294.7	295
2	1501 + 4 % C	0.15	560	10–15	10	441.8–447.1	443.8
3	1501 + 4 % C	0.3	560	10–15	10	199.4–237.0	226
4	1501 + 4 % C	0.45	560	10–15	10	167.3–234.6	210

all the cases, only the single pores are revealed at the line of composite contact with the interlayer. From the data of X-ray microanalysis the diffusion of magnesium into intermediate layer for up to 6 μm depth is observed (see Figure 4).

As is seen from Table 2, the higher strength and stable repetition of results are attained in bonding of CM 1501 + 4 % C at an 0.15 mm initial thickness of the interlayer. Increase in interlayer thickness up to 0.30 and 0.45 mm leads to the reduction of strength characteristics. This is explained by the fact that the contact strengthening of a soft interlayer at static tensile tests is realized to a less degree in the joint at thickness of the interlayer at the interface of higher than 250–300 μm, than in case of using thinner interlayers. Static tensile strength in joints of composite 1501 + 4 % C at optimum conditions of diffusion bonding reached 443.8 MPa, that is amounted to 88 % of the parent metal strength. Fractures in all the cases were in bond.

CONCLUSIONS

1. Structure and properties of dispersion-strengthened composite materials 1013 + 4 % C and 1501 + 4 % C and their joints, produced by diffusion bonding in vacuum, were studied. It was established that composites are characterized by a fine-grain structure of the matrix (size of structural elements is 0.2–0.5 μm), high density of dislocations ($9.5\cdot10^{10}$–$1\cdot10^{11}$ cm^{-2}) and dispersity of strengthening phase precipitations Al_4C_3 (0.02–0.13 μm), that stipulates increased strength, rigidity and thermal stability of the material.

2. Technology of diffusion bonding in vacuum with a thermodeformational cycling has been developed which makes it possible to produce the quality joints owing to the intensification of plastic deformation of a soft interlayer in the butt.

3. Strength of joints for CM 1013 + 4 % C of 295 MPa and for CM 1501 + 4 % C of 443.8 MPa was obtained under the optimum conditions.

1. (1985) *Composite materials*. Refer. Book. Ed. by D.M. Karpinos. Kyiv: Naukova Dumka.
2. Toshio, E., Kenji, J., Votaro, M. et al. (1987) Diffusion bonding of A6063 aluminum alloy reinforced with aluminia short fibre. *Quart. J. Jap. Weld. Soc.*, **3**, 31–37.
3. Bushby, R.S., Scott, V.D. (1995) Joining of particulate silicon carbide reinforced 2124 aluminum alloy by diffusion bonding. *Mat. Sci. and Techn.*, **8**, 753–758.
4. Escalera, M.D., Urena, A., de Salazar, G.J.M. (1997) Solid state diffusion of A6061 matrix composites reinforced with aluminia particles. In: *Proc. of Int. Europ. Conf. on Welding and Joining Science and Technology*, Madrid, March 10–12, 1997.
5. Ryabov, V.R., Kharchenko, G.K., Markashova, L.I. et al. (1996) On the weldability of dispersion strengthened composite (Al + 4 % C). In: *Proc. of Int. Welding Conf.*, Slovakia, March 5–7, 1996.
6. Markashova, L.I., Ryabov, V.R., Statsenko, V.V. et al. (1995) Study of structure of dispersion-strengthened composite material Al + 4 % C. *Avtomatich. Svarka*, **6**, 21–26.
7. Karakozov, E.S. (1986) *Pressure welding of metals*. Moscow: Mashinostroenie.

EFFECT OF HYDROSTATIC PRESSURE ON ARC STABILITY IN UNDERWATER WELDING (Review)

Yu.Ya. GRETSKY and **Yu.S. MAKSIMOV**
E.O. Paton Electric Welding Institute, NASU, Kyiv, Ukraine

The problem of ensuring stability of the arc burning in water under conditions of high ambient hydrostatic pressure is considered. Current notions of causes of instability of the arc discharge are presented. Input principles are formulated for arrangement of studies to be conducted under the above conditions to solve the problem of expansion of technological capabilities of the method of mechanised underwater flux-cored wire welding developed by the E.O. Paton Electric Welding Institute.

Keywords: *underwater welding, hydrostatic pressure, arcing, process stability*

Ensuring a stable arc is one of the key problems of developing electrode materials, as well as developing or improving a welding process. This problem is particularly topical for underwater welding performed by the so-called «wet» method, where the arc burns directly in water without any artificially made physical barrier to protect the welding zone from an adverse effect of the environment.

Behaviour of the welding arc and character of melting of the electrode metal in welding performed in water are substantially different from those in welding performed in air [1, 2]. During welding performed directly in water the arc burns in a vapour-gas bubble which surrounds it and thus creates conditions required for its existence. The vapour of water at high temperatures of the arc gap dissociates to form hydrogen and oxygen. Presence of these gases has a decisive effect on the arc stability and transfer of the molten metal. Oxygen, being a surface-active element, favours refining of the drops of molten metal because of reduction in its surface tension. At the same time, hydrogen constitutes the major portion of volume of the vapour-gas atmosphere. Owing to its increased thermal conductivity and high ionisation potential, it initiates contraction of the arc column and causes increase in the electrodynamic force that affects a molten metal drop on the side of the arc, keeping it at the electrode tip. Thus, hydrogen increases size of the drops transferred to the pool. It is a known fact that, as the depth of submergence (hence, hydrostatic pressure) increases, the degree of oxidation of the weld metal dramatically grows, which is indicative of a more intensive process of fixation of oxygen. This leads to increase in a partial pressure of hydrogen within the welding zone.

The results of studies [3] simulating conditions of wet welding at a depth of 50 m show that growth of the hydrostatic pressure is accompanied by a substantial increase in duration and frequency of short circuits (Figure 1). This leads to a higher risk of extinction of the arc and a marked deterioration of stability of the process. Based on analysis of experimental data, the authors of that study claim short circuits taking place at substantial depths are of two types: short circuits resulting from increase in size of the drops (the main cause in this case is growth of the partial pressure of hydrogen), and short circuits resulting from short-time contacts of the electrode wire tip with the pool surface caused by the arc extinction. Share of the second type of short circuits increases with increase in the depth of submergence.

The fact of increase in the arc extinction with growth of the pressure, proved by analysis of histograms of current and voltage, explains a substantial growth of the arc voltage at large depths as registered by researchers [4]. Fixation of the process parameters using conventional devices yielded a mean value of the arc voltage that grows as a result of increase in share of the open-circuit voltage at the moments of the arc extinction. G. Coriatt [5] attributes shifting of the ranges of values of the stable welding arc parameters towards increased values of the arc voltage and decreased values of the welding current (Figure 2) to a high ionisation potential of oxygen. As

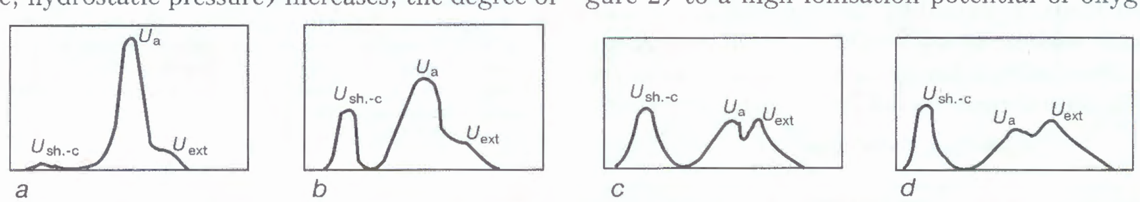

Figure 1. Histograms of arc voltage U_a in wet flux-cored wire welding at depths of 0.5 (*a*), 10 (*b*), 20 (*c*) and 50 (*d*) m ($U_{sh.-c}$ — short-circuit voltage, U_{ext} — arc extinction voltage)

seen from the Figure, the ranges of values of the said parameters become substantially narrower with increase in pressure (depth), which makes the problem of ensuring stability of the wet welding process much more difficult [6].

Another factor which is characteristic only of the process of wet welding and has a negative effect on the arc stability is fluctuation of the vapour-gas bubble volume. Alternation of the processes of growth of the bubble to a critical size and collapse with floating of its major part (50–80 %) occurs at a frequency of 10–15 cycle/s on the average [7]. It is the opinion of the authors of study [8] that collapse of the bubble causes deviation or even extinction of the arc.

The effect of depth results from decrease both in size of the vapour-gas bubble and in length of the arc at a constant voltage. The first factor can be eliminated by counteracting the hydrostatic pressure through increasing the amount of gas-forming components in the wire charge composition, while the second factor can be eliminated by raising the arc power from a power supply (mainly through increasing the voltage). The latter should lead to increase in the arc gap and, therefore, reduce the probability of short circuits.

An effective method is to change the ionisation potential or realise the combined impact by gas-forming and ionising components. Analysis of the above approaches on the basis of available literature data will make it possible to choose one of them to solve the scientific problem of stabilisation of the arc process.

Study [9] considers energy parameters of the arc burning in water under a pressure of 5 MPa, which is equivalent to the hydrostatic pressure of water in wet welding performed at a depth of down to 500 m. The experimental procedure employed provided for the use of standard welding consumables, i.e. solid wire Sv-08A (C < 0.08 %) with a diameter of 3 mm and special flux-cored wire PPS-AN1 (0.09–0.1 % C) with a diameter of 1.6 mm [10]. The authors of study [9] used these consumables to find the values of voltage and current to provide the stable arc in the above range of the pressure. Results of processing of the experimental data are shown in Figure 3.

They evidence that the open-circuit voltage of the power supply and current of such arcs grow very intensively and approximately in proportion to the pressure of water. So, for actual depths of the coastal shelf (100–300 m) the value of the open-circuit voltage should be not less than 120–180 V, and the arc current in this case should be 600–1000 A. The result obtained shows that only in a high-current plasma of the arc column the pressure is sufficient to oppose the hydrostatic pressure of water. But this gives ground to seriously doubt the possibility of realising a deep-water wet mechanised welding using available electrode wires only through developing the specialised high-capacity power units with a high value of the open-circuit voltage, as this may lead to the risk of an electric shock to a welding diver and involves vio-

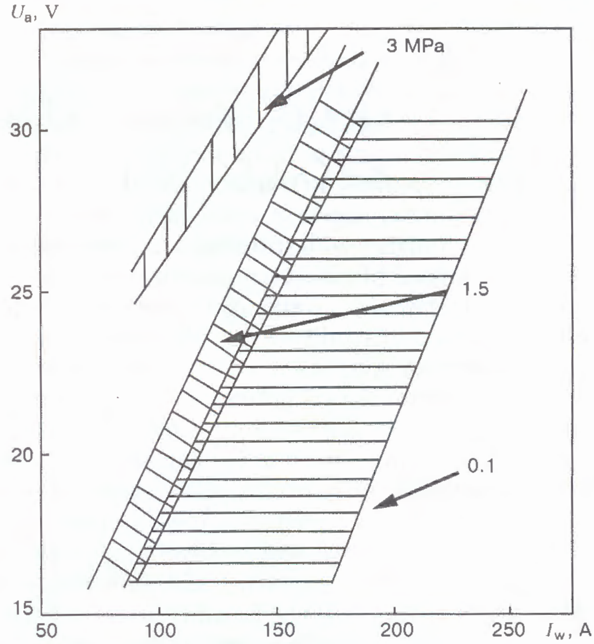

Figure 2. Effect of hydrostatic pressure on position of the range of acceptable values of arc voltage U_a and welding current I_w in wet welding using stick electrodes [5]

lation of international standards specifying labour conditions for humans working under water.

Apparently, the metallurgical way of handling this problem is more practicable. It is supported also by the data proving that the addition of an experimental master alloy containing rare-earth metals to a flux-cored wire of the PPS-AN1 grade allowed some stabilisation of the arc at a depth of 40–50 m [3] and enabled stability of the arc in welding using stick electrodes to be maintained at a depth of down to 150 m [11].

It is reported [12] that the use of electrodes of the E7014 type (according to the AWS A5.1 specifications) with a waterproof coating allowed the arc to be maintained and even a joint to be produced by welding under actual conditions of the Gulf of Mexico at a depth of 185 m (560 feet). But to say the truth,

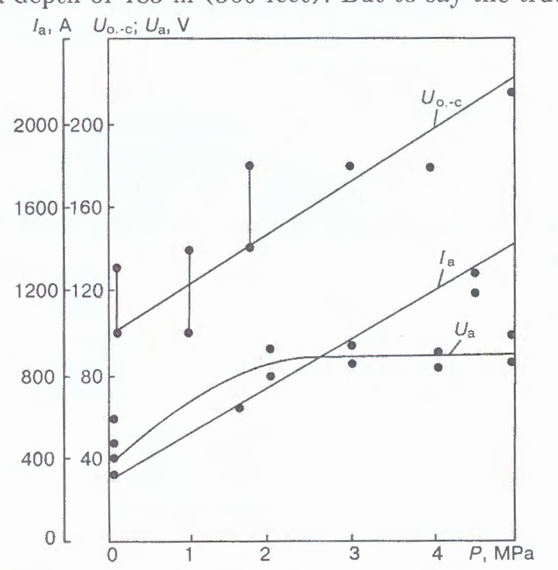

Figure 3. Dependence of main parameters of the stable arc upon the hydrostatic pressure in the experiment by G.I. Leskov [9]

the quality of that joint was rather low because of a continuous porosity and heavy oxidation of the weld metal, as well as an incomplete fusion with the base metal.

The stable state of the arc discharge, i.e. the state of the sustained arcing with no deviations from the assigned conditions and no transitions of the discharge to the other forms, depends upon many factors. In this case the indispensable condition is the presence of a highly ionised plasma between the electrodes. It is known [13] that an effective method to keep to this condition is to add readily ionisable components to the arc. Note that even the traces of materials with a low value of the ionisation potential deposited on the electrodes provide a marked improvement in the arc stability. The refined method for calculation of the ionisation potential of multicomponent systems with activating additions is described in [14], and examples of application of mechanised arc welding using an electrode wire with the activating additions are given in [15]. Reportedly [16], the possibilities of controlling the technological properties of the arc can be widened by increasing the amount of activators per unit weight of the wire. Increase in the amount of the activators leads to decrease in difference between the arcs at straight and reverse polarity of the current. Salts of alkali and alkali-earth metals, such as sodium, potassium, caesium, strontium, calcium etc., are usually used as the activators.

It is believed that the fact of a more successful application of manual welding for stabilisation of the arc under conditions of the increased hydrostatic pressure, compared with flux-cored wire welding, can be attributed to the presence in the electrode coating of at least one component that favours to a considerable degree ionisation of the arc gap and is absent in the composition of the flux-cored wire charge. To begin with, this could be sodium silicate which is necessarily used for the fabrication of material for the electrode coating. Marble, i.e. a chemical compound on the alkali-earth metal base, which is susceptible to dissociation to form gas, may also be helpful.

Utilisation of flux-cored wire PPS-AN1 and its improved modification PPS-AN2 (TUU 05416923.039–98) developed by the E.O. Paton Electric Welding Institute for mechanised wet welding provides a stable arc, satisfactory weld formation and required level of mechanical properties of welded joints made at a depth of 20 m. At the same time, the range of depths at which underwater structures are usually located (pipelines, stationary foundations of off-shore platforms etc.) in the coastal shelf zone is much deeper than 50–300 m. Therefore, at present the technological capabilities of the method of mechanised underwater welding are considerably limited.

The above estimates and considerations were used as the basis for the program of experimental studies aimed at evaluation of the effect of readily ionisable and gas-forming additions to the flux-cored wire charge on stabilisation of the arc under conditions of an increased pressure of water surrounding the arc.

1. Chon-Liang Tsai, Masubushi, K. (1977) Interpretive report on underwater welding. *Welding Research Council Bull.*, **224**, 37.
2. Masubuchi, K. (1981) Underwater factors affecting welding metallurgy. In: *Proc. of Int. Conf. on Underwater Welding of Offshore Platforms and Pipelines*, New Orleans, Nov. 5–6, 1980. Miami: AWS.
3. Pokhodnya, I.K., Gorpenyuk, V.N., Kononenko, V.Ya. et al. (1990) Some peculiarities of arc burning and metal transport in underwater welding with flux-cored wire. *Avtomatich. Svarka*, **9**, 1–4.
4. Lebedev, V.K., Leskov, G.I., Uzilevsky, Yu.A. (1980) Calculation of principal characteristics of arc in underwater mechanised welding. In: *Underwater welding and cutting of metals*. Ed. by A.E. Asnis. Kyiv: PWI.
5. Coriatt, G. (1979) Repairing deep-sea pipelines and structures. *Welding Design and Fabrication*, July, 60–64.
6. Ibarra, S., Liu, S., Olson, D.L. (1995) Underwater wet welding of steel. *Welding Research Council Bull.*, **401**, 39.
7. Madatov, N.M. (1965) Properties of vapour-gas bubble around the arc in underwater welding. *Avtomatich. Svarka*, **12**, 25–29.
8. Rehfeldt, D., Bollmann, A., Korbe, T. (1989) Statistical analysis for monitoring underwater arc welding process. In: *Proc. of Int. Conf. on Welding under Extreme Conditions*, Helsinki, Sept. 4–5, 1989. Oxford: Pergamon Press.
9. Leskov, G.I., Potikha, O.M. (1999) Arc energy parameters under conditions of hydrostatic pressure of up to 5 MPa. *Avtomatich. Svarka*, **1**, 15–18.
10. (1980) *Flux-cored wires for arc welding*. Ed. by I.K. Pokhodnya. Kyiv: Naukova Dumka.
11. Scelagowski, P. (1985) Verfahrenstechnische Entwicklung beim Unterwasserschweissen. *Schweissen und Schneiden*, **37**, 108–111.
12. Wood, B.J., Bruce, W.A. (1991) Underwater wet repair welding at depths approaching — 600 ft. In: *Proc. of Int. Conf. on Underwater Welding*, New Orleans, March 20–21, 1991. Miami: AWS.
13. Leskov, G.I. (1989) *Electric welding arc*. Moscow: Mashinostroenie.
14. Voropaj, N.M., Krivtsun, I.V. (1978) Effective potential of ionisation of multi-component systems with activating additives. *Avtomatich. Svarka*, **2**, 66–67.
15. Paton, B.E., Voropaj, N.M. (1979) Shielded-gas activated consumable electrode welding. *Ibid.*, **1**, 1–7, 13.
16. Lenivkin, V.Kh., Dyurgerov, N.G., Sagirov, Kh.N. (1989) *Technological properties of the welding arc in shielding gases*. Moscow: Mashinostroenie.

APPLICATION OF FLUX IN MIG WELDING OF THIN-SHEET ALUMINIUM ALLOYS

R.M. SAIDOV[1], **U. SEMMLER**[2], **K.-J. MATTHES**[2] and **S. THURNER**[2]
[1]State Technical University, Tashkent, Uzbekistan
[2]Chemnitz Technical University, Germany

Results of investigation of arc consumable electrode inert gas welding of thin-sheet aluminium alloys using a cleaning and forming flux are presented. It is shown that the use of flux in welding aluminium alloy AlMg4.5Mn (5083) promotes producing of welded joints of a high quality and level of mechanical properties.

Keywords: *arc welding, aluminium alloys, welded joints, consumable electrode, flux, inert gas, oxide films, equal strength of weld and parent metal*

At present, one of the most spread methods of welding aluminium structures and products in industry is an argon arc consumable electrode welding [1–5]. However, the presence of defects in welds using this method, such as oxide inclusions, porosity, poor formation of reverse side of welds and others, is observed, thus decreasing the mechanical and service properties of joints, in particular in critical structures and products. The known technologies of welding, which apply different technical solutions (special backings, magnetic stirring of weld pool, pulsed power sources, argon blowing, etc.), do not eliminate, as a whole, all the problems of aluminium alloy welding.

The investigations, which were carried out, showed that one of the most effective methods of improving the quality of welded joints, made from aluminium and its alloys, is the use of a cleaning and forming flux. The application of flux promotes the reduction in weld defects, improvement of weld root formation and protection of a back bead from surrounding medium effect, that, respectively, improves the mechanical and service properties of welded joints.

The investigations were performed on aluminium alloy AlMg4.5Mn (5083), used widely in welded structures and products in Europe, USA and Japan. Chemical composition of this alloy is given in Table 1 and corresponds to standards of DIN EN 573.

Investigation of flux effect on the quality and properties of welded joints was made on welding plates of 2, 3 and 4 mm thickness. The flux of TFA-12 grade, consisting of fluoride and chloride salts of alkali and alkali-earth metals, was used as a cleaning and forming flux [6]. It was deposited in the form of a paste (mixture of flux powder with acetone or alcohol) of 0.2–0.4 mm thickness and 5–8 mm width on a reverse side of edges being welded using a brush or aerosol high-pressure bottle.

The 300×150 mm plates were butt welded in the equipment for the automatic argon arc consumable electrode welding CLOOS GLS 503 QUINTP Version Profi, V1.60 in a pulsed condition using 1.2 mm diameter electrode wire from alloy 5087. Chemical composition of electrode wire is given in Table 1 and corresponds to standards of DIN EN 485.

To evaluate the flux effectiveness, the plate edges being welded were not subjected to chemical etching and mechanical cleaning before welding. Welding conditions were optimized preliminary for welding alloy AlMg4.5Mn using a conventional technology without a cleaning and forming flux (Table 2). Optimum conditions were defined by the uniformity and quality of weld formation from the side of welding and back bead.

To detect the internal and external defects, the samples after welding were subjected to X-ray control. The contamination of welds with oxide inclusions was evaluated by their relative extension:

$$\Sigma l_o / l_j,$$

where Σl_o is the total extension of oxide inclusions in weld; l_j is the weld length.

The evaluation of flux effect on geometry of welds was also made. For this, the width b and sagging of back bead K_p of weld h were measured (Figure 1). Abrupt transition from weld metal to the parent metal

Table 1. Chemical composition of AlMg4.5Mn alloy and electrode wire of alloy 5087

Material	Elements, wt.%							
	Si	*Fe*	*Cu*	*Mn*	*Mg*	*Cr*	*Zn*	*Ti*
AlMg4.5Mn (5083)	0.40	0.40	0.10	0.4–1.0	4.0–4.9	0.05–0.25	0.25	0.15
Alloy 5087	0.25	0.40	0.05	0.7–1.1	4.5–5.2	0.05–0.25	0.25	0.15

Table 2. Optimum conditions of argon arc welding of aluminium alloy plates

Thickness, mm	I_{base}, *A*	I_{eff}, *A*	U_p, *V*	U_{eff}, *V*	v_w, *cm/min*	v_f, *cm/min*	F_p, *Hz*	t_p, *ms*	Q_{Ar}, *l/min*
2.0	62	102	27	18.5	125	560	80	1.45	12
3.0	62	102	27	18.5	70	560	80	1.45	12
4.0	62	102	27	18.5	40	560	80	1.45	12

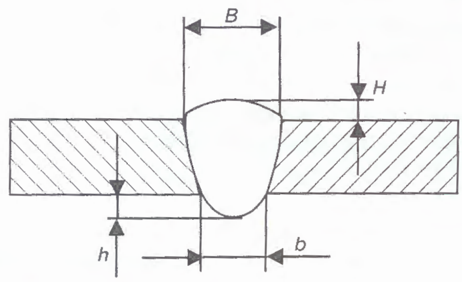

Figure 1. Sketch of weld

was evaluated by the coefficient of penetration shape K_p which was determined by formula

$$K_p = b/h.$$

The higher the value of this coefficient, the smoother transition from the deposited metal to the parent metal and better quality of the weld back bead formation. Uniformity of back bead sagging was evaluated by value Δh, which was determined from the difference of maximum h_{max} and minimum h_{min} value of the back bead sagging:

$$\Delta h = h_{max} - h_{min}.$$

The non-uniform back bead sagging has a negative influence on the service characteristics of welded joints of structures and products operating under the conditions of dynamic loads. Metallographic examinations and mechanical tests of welded joints were made.

Welded joints, produced in consumable electrode argon arc pulsed welding without the use of flux, have a dark oxidized color from both sides of the weld (Figures 2, *a* and 3, *a*). The use of flux makes it possible to obtain a light and smooth surface of welds (Figures 2, *b* and 3, *b*) by the removal of oxide films, covering the surface of edges being welded and reliable protection of weld surface from oxidation during welding and weld cooling. In places of flux entering the butts of edges at its deposition before welding, the surface contamination is occurred, not influencing the weld quality. Remnants of the flux and slag are well removed during washing by a running water.

From the side of back bead the weld, produced by the conventional technology, has a dark and oxidized rough surface (Figure 3, *a*), while the weld, produced with a flux, has a smooth and glittering surface after washing by a running water of the flux and slag remnants (Figure 3, *b*).

With increase in thickness of metal being welded the weld appearance from the side of welding with a flux, becomes lighter and smoother. This is explained by the decrease in welding speed that contributes to the complete treatment of the weld pool molten metal with the flux. Here, the weld appearance from the back bead side made with the use of flux does not depend on the thickness of metal being welded and has a smooth and glittering surface.

One of the drawbacks of welding the aluminium alloys is the poor formation of the weld back bead. Due to a high fluidity of the weld pool the process of welding without any backings becomes complicated. The back bead is flaky with an abrupt transition to the parent metal (Figure 4, *a* and *b*). Abrupt transition plays a role of stress raiser that reduces the serviceability of welded joints, at dynamic loads in particular.

The investigation of cross sections of welded joints made by consumable electrode argon pulsed arc welding using the conventional technology and with the use of a cleaning and forming flux showed that the use of flux in welding influences favorably the shape and sizes of welded joints (Figure 4 *b*, *d* and Figure 5).

The favourable effect of the flux on the weld penetration shape is proved by the higher values of the coefficient of penetration shape K_p (Figure 6, *a*) characterizing a smooth transition from the weld metal to the parent metal. Moreover, the reduction in efficiency of flux effect on the formation of weld penetration shape is observed with increase in thickness of metal being welded.

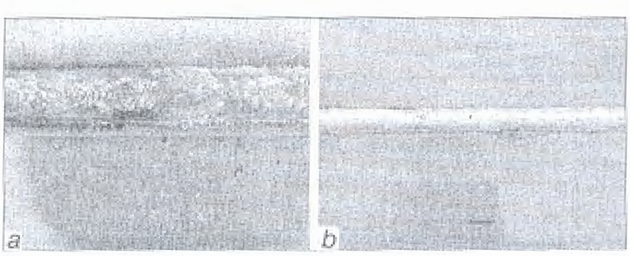

Figure 2. Appearance of 4 mm thick AlMg4.5Mn alloy welded joints made by welding using a conventional technology (*a*) and with a flux (*b*) from the side of welding

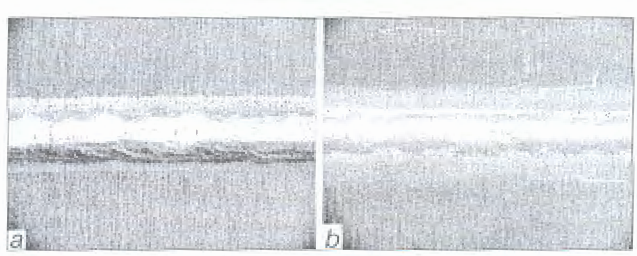

Figure 3. Appearance of 4 mm thick AlMg4.5Mn alloy welded joints made by welding using a conventional technology (*a*) and with a flux (*b*) from the side of weld back bead

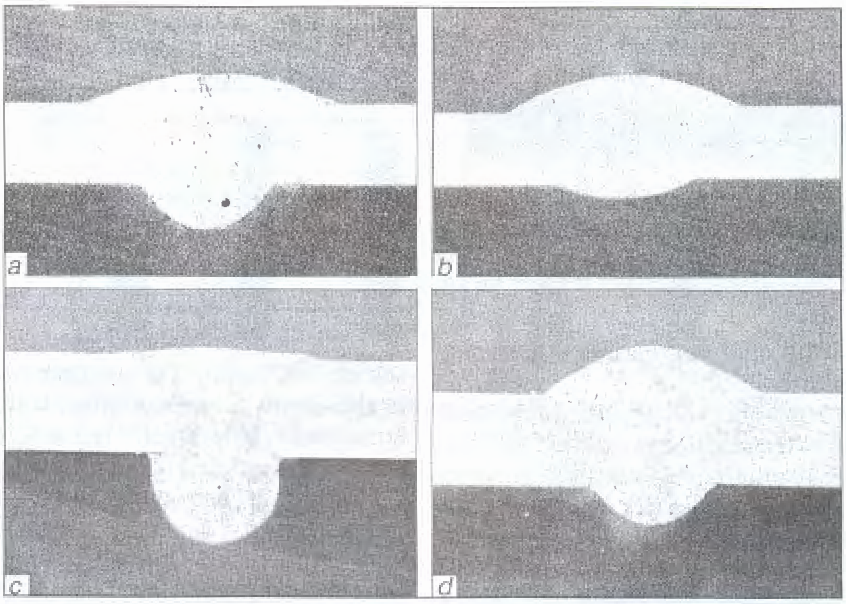

Figure 4. Macrosections of welded joints of AlMg4.5Mn alloy of 2 (*a*, *b*) and 4 (*c*, *d*) mm thickness made by a conventional technology (*a*, *c*) and with use of cleaning and forming fluxes (*b*, *d*)

The use of the flux can also provide the weld back bead with a more uniform formation. This can be judged from the value of a non-uniformity Δh of weld penetration, which is much lower than in welds made with the flux use (Figure 6, *b*). Increase in thickness of metal being welded does not almost influence the uniformity of penetration of weld produced in welding using a flux.

Improvement of formation of the back bead of aluminium alloy welds can be explained by the fact that the flux removes oxide films covering the metal edges being welded and contributes to the improvement of wettability of the parent metal with a weld pool molten metal because of a decrease in interphase tension between molten and solid metal. Besides, a liquid flux interlayer plays a role of an elastic support

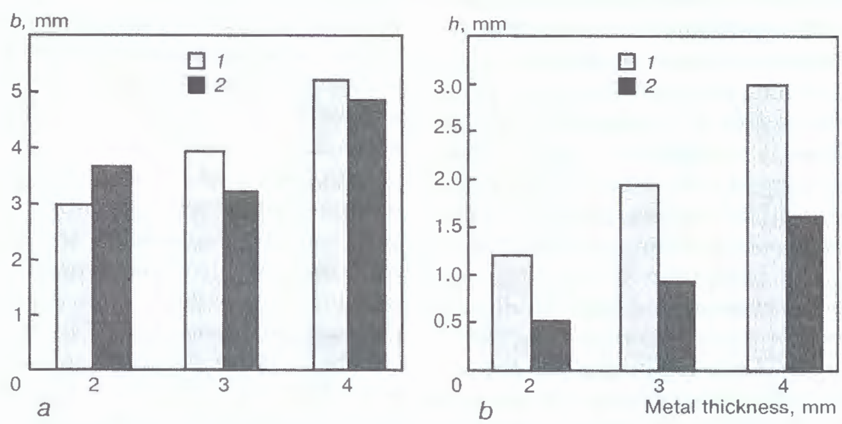

Figure 5. Width (*a*) and back bead sagging *h* of welds (*b*) depending on thickness of metal being welded and conditions of welding without (*1*) and with flux (*2*)

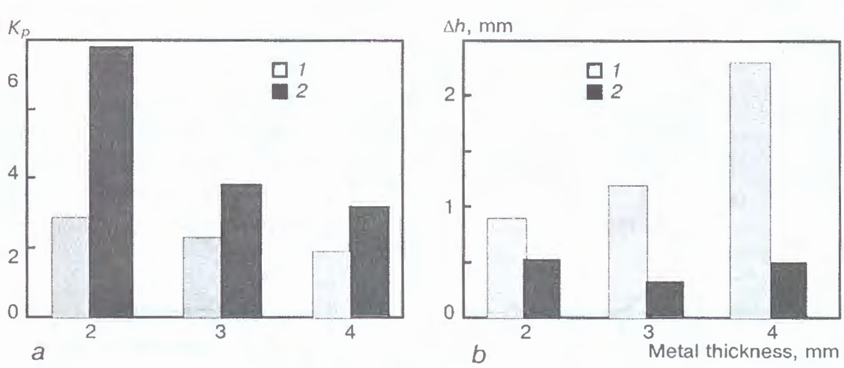

Figure 6. Dependence of coefficient of penetration shape K_p (*a*) and non-uniformity of penetration Δh of weld (*b*) on thickness of metal being welded and welding conditions without (*1*) and with flux (*2*)

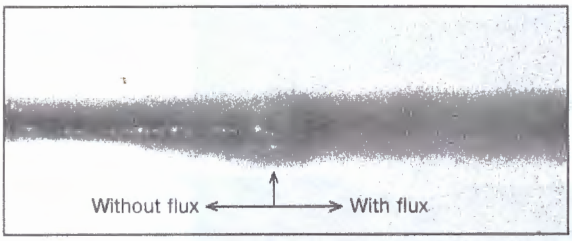

Figure 7. X-ray photograph of 2 mm thick AlMg4.5Mn alloy welded joint made by a conventional technology and with the use of flux

Table 3. Effect of product surface condition and welding conditions on mechanical properties of welded joints of 3 mm thick alloy AlMg4.5Mn

Surface preparation before welding	*Welding conditions*	*Mechanical properties*	
		σ_t, *MPa*	δ, *%*
Cleaning by metallic brush	Without flux	$\frac{313-320}{316}$	$\frac{25-27}{26}$
Without cleaning	With flux	$\frac{313-317}{315}$	$\frac{26-41}{31}$

and maintains the weld pool molten metal from sagging and formation of burnouts.

Results of X-ray control of the welded joints made by the consumable electrode argon arc pulsed welding using a conventional technology showed the presence of a large amount of internal defects in welds in the form of oxide inclusions and pores. The use of the cleaning flux in welding reduces the amount and sizes of pores in welds made from the aluminium alloys. Coarse porosity (of not less than 100 μm diameter), which is mainly arranged on oxide inclusions, is eliminated completely with the use of the flux. These pores are easily revealed by X-ray control of weld metal and depend on the amount of oxide inclusions in the weld metal (Figure 7).

The investigations showed that the amount of pores is reduced significantly both with the increase in thickness of metal being welded and also with the use of a cleaning and forming flux (Figure 8). This effect is, probably, explained by the fact that welding of 3 and 4 mm thick plates (Table 2) was realized at welding speeds which provided conditions for a complete removal of oxide inclusions and pores by the flux.

The abrupt suppression of the pore formation process in aluminium alloy welds is explained by several reasons which are greatly interrelated. This process depends on oversaturation of molten metal with gases and conditions of initiation and propagation of gas bubbles [7]. In welding using a cleaning flux a reliable protection of weld back bead from surrounding medium is attained and, consequently, the conditions are created for reduction in weld pool molten metal ovesaturation with gases. Decrease in oxide inclusions (Figure 8), mainly in the form of oxide films, promotes the reduction in amount of moisture entered the molten metal. The another positive contribution to the decrease in oxide films and other non-metallic inclusions is a significant reduction in ready interfaces causing the initiation and propagation of gas bubbles.

Results of mechanical tests of AlMg4.5Mn alloy welded joints with a removed reinforcement of welds in welding with a flux use are presented in Figure 9 (mechanical properties of parent metal in accordance with DIN EN 485-2: $R_m = 275$–350 MPa, $\delta_{min} = 15$ %). According to the results obtained the tensile strength of welded joints made by a conventional technology and with the use of flux are similar for 2 and 3 mm thicknesses and it is increased for welded joints of 4 mm thickness, made with the flux use (Figure 9).

The results obtained showed that the application of the flux in welding does not decrease the mechanical properties of welded joints, and in some cases it even increases them. The larger thickness of metal being welded, the higher effect of flux on the mechanical properties. This is associated with the fact that with increase in plate thickness the welding speed is decreased, that creates the conditions for more effective metallurgical treatment of molten metal of the weld pool with the flux and contributes to producing of more quality welded joints.

The quality of the welded joints, made from aluminium alloys, especially alloys with a high magnesium content, depends on the surface condition of edges being welded. This is explained by the fact that the aluminium alloys, containing more than 1.5 % Mg, form the oxide film of MgO at the surface, which adsorbs moisture from the surrounding medium and forms $Mg(OH)_2$ [8]. With time this film has a tendency to the growth and can have a thickness up to

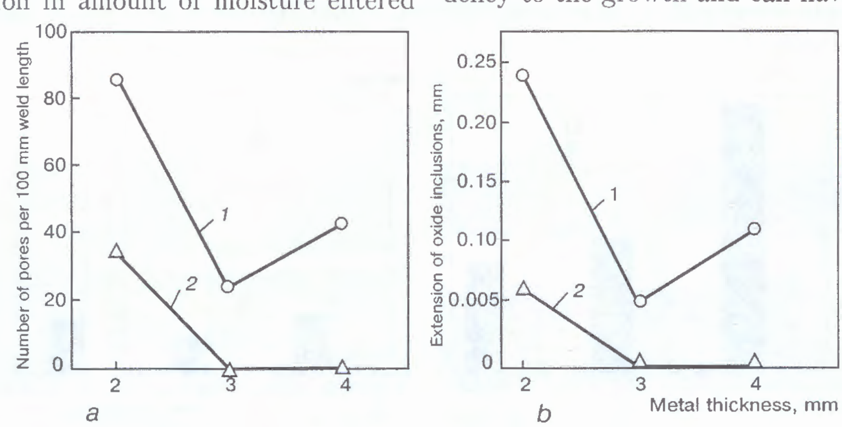

Figure 8. Dependence of number of pores (*a*) and extension of oxide inclusions (*b*) on the thickness of metal being welded and welding conditions in AlMg4.5Mn alloy welds

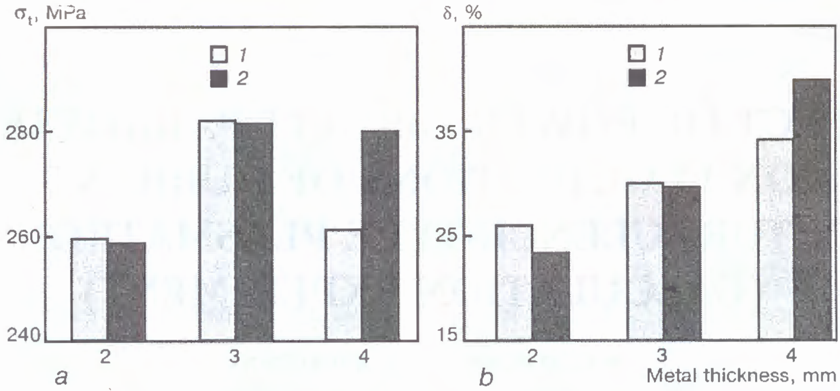

Figure 9. Tensile strength σ_t (*a*) and elongation δ (*b*) of AlMg4.5Mn alloy welded joints depending on thickness of metal being welded and welding conditions without (*1*) and with flux (*2*)

100 μm [9]. During welding the oxide film, covering the edges being welded, contributes to the formation of oxide inclusions and coarse porosity, which are formed as a result of formation of hydrogen, the product of decomposition of magnesium hydroxide. Existing technological instructions on welding aluminium alloys recommend the obligatory preliminary removal of oxide films before welding. Usually, the chemical treatment of surface of products or mechanical cleaning of edges by a metallic brush are performed.

The use of a cleaning flux in aluminium alloy welding makes it possible to minimize the requirements to the surface condition of the products, i.e. it is possible to perform welding without the preliminary cleaning of edges being welded or to clean them by a metallic brush from the side of welding. Results of investigation of effect of product surface condition on the mechanical properties of welded joints from the aluminium alloy AlMg4.5Mn (without removal of weld reinforcements), obtained in welding using a conventional technology with the use of a cleaning flux, are given in Table 3.

The results obtained showed that the application of fluxes in welding products without preliminary chemical or mechanical treatment of edges being welded can provide welds of the good quality and mechanical properties, equal in strength to welds, made by a conventional technology with the preliminary cleaning of surface of edges being welded. The similar effect is attained due to the fact that the flux during welding contributes to the removal of oxide films from the edges being welded, thus preventing their enter the weld pool and protecting molten metal from the further oxidation during welding and crystallization of weld metal.

It can be outlined in the conclusion that the use of a cleaning flux makes it possible to improve the appearance of welded joints, characterized by a smooth and glittering surface, to contribute to improving the wettability of the parent metal with a weld pool molten metal, that, consequently, reduces the interphase tension between the liquid and solid metal. The liquid flux interlayer plays a role of an elastic support and maintains the weld pool molten metal from sagging and formation of burnouts. The application of flux promotes an abrupt reduction in oxide inclusions and porosity in welds made from alloy AlMg4.5Mn. Reduction in porosity is explained by that the flux removes the oxide films, on which the moisture is adsorbed, being a source of pores, by binding of hydrogen with fluorides included into flux composition and by protection of weld back bead from the effect of the surrounding medium. The use of the flux does not deteriorate the mechanical properties of welded joints, and in some cases it even increases them. The requirements to the preparation of edges before welding are minimized, i.e. the feasibility appears to eliminate the preliminary chemical or mechanical cleaning of the surface.

1. Brockmann, G.J. (1997) Joining of heat-exchangers for the automotive industry. In: *Proc. of IIW Seminar on Trends in Welding of Lightweight Automotive and Railroad Vehicles*, Febr. 26–28, 1997.
2. Matthes, K.-J., Lang, H. (2000) Fuegen von Aluminiumschaeumen mit porositaetsbildenden Zusatzwerkstoffen. *DGM-Symp. Metallschaeume*, Wien, Febr. 28–29, 2000. Wienheim: Willey-VCH.
3. Brunnhuber, D., Brandt, H., Schmidt, H. (2001) *Aluminium welding in shipbuilding. The manufacture of marine gearbox casings with welding consumables and pulsed current power sources from ESAB*, 56(**2/3**), 19–20.
4. (2001) Schweisstechnische Spitzenleistungen in der Motorradfertigung. *Aluminium*, 77(**6**), 482–495.
5. Irving, B. (2000) The autoindustry gears up for aluminium. *Welding J.*, 79(**11**), 63–68.
6. Saidov, R.M. *Welding flux*. Int. Pat. PCT/UZ98/00001.1998. Publ. 24.09.98. Europ. Pat. EP1083021. Publ. 14.03.01.
7. Pokhodnya, I.K. (1972) *Gases in welds*. Moscow: Mashinostroenie.
8. Kurdyumov, A.V., Inkin, S.V., Chulkov, V.S. (1980) *Filtering of aluminium melts*. Moscow: Metallurgiya.
9. Saidov, R.M. (1984) *Influence of flux paste on quality and properties of welded joints from aluminium alloys*. Syn. of Thesis for Cand. of Techn. Sci. Degree. Tashkent.

EFFECT OF POWER CIRCUIT PARAMETERS ON FLUCTUATIONS OF CURRENT IN TURBULENCE-TYPE PLASMATRONS (CALCULATION EXPERIMENT)

V.L. DZYUBA and **G.S. KALYUZHNY**
V. Dal East-Ukrainian National University, Lugansk, Ukraine

Dependence of values of large-scale current fluctuations in turbulence-type plasmatrons upon the power circuit parameters has been studies by the method of a calculation experiment. As shown by its results, the value of the arc current fluctuations first decreases with increase in the natural frequency of the power circuit, and then remains approximately at a constant level that lowers with increase in circuit inductance.

Keywords: *plasmatron, arc current stabilisation, large-scale fluctuations, arc shunting, calculation experiment*

Burning of the DC arc in the plasmatron work chamber is a non-stationary process. One of the main reasons of this non-stationarity is an irregular variation in the arc length caused by drift of its radial region with a gas flow and subsequent breakdown between the arc and the chamber wall (shunting) [1–4]. This leads to formation of large-scale fluctuations of the voltage and arc current, the frequency of which is 1–10 kHz, while the spread of a variable component of voltage may amount to 50 % of its mean value [2].

Burning of the arc in the turbulence-type plasmatrons occurs in a highly turbulent flow, especially in a region where the gas layer heated by the electric arc adjoins the turbulent boundary layer growing on the channel walls. This induces high transverse fluctuations of the arc leading to decrease in the breakdown voltage, and the shunting process in this case takes up a clearly defined random character [1].

This circumstance makes analysis of the shunting process difficult, and studies dedicated to investigation of this process are mostly of an experimental character [1–3]. At the same time, it is apparent that the problem of diminishing the effect of the shunting process on the arc current and its stabilisation is of a high practical importance.

This study is an attempt to investigate dynamics of development of large-scale disturbances of the arc current by using a calculation experiment. Quantitative characteristics of disturbances of the current have been determined, and the possibility of an optimal selection of the power circuit parameters aimed at reduction of these disturbances has been considered.

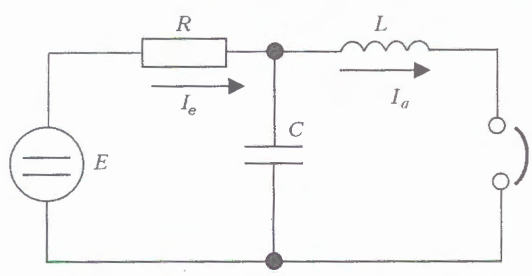

Figure 1. Equivalent electric circuit of the power supply–arc system (see designations in the text)

Mathematical model. *Equation for arc current fluctuations*. Consider the mathematical model of disturbances of the arc current for a typical power circuit of the plasmatron shown in Figure 1 [1, 2]. The circuit comprises power supply with voltage E, ballast resistance R, inductance L and capacitance C, the values of which are affected also by the elements of the arc ignition circuit. The most applicable method for the arc ignition is that by using an oscillator [1]. Internal resistance of the power supply is assumed to be equal to zero.

Determine relationship between the current and voltage for the circuit elements using the Kirchhoff's equation:

$$I_e = CU_C' + I_a; \quad U_C = LI_a' + U_a; \quad E = I_eR + U_C,$$

where indices e, a and C relate to the power supply, arc and capacitor, respectively. The primed symbols designate time derivatives.

The transformations yield:

$$I_a'' + \frac{1}{RC} I_a' + \frac{1}{LC} I_a = \frac{E}{RCL} - \frac{U_a}{RCL} - \frac{U_a'}{L}. \quad (1)$$

Values U_a and I_a are related via a volt-ampere characteristic of the arc.

Add value

$$\omega = \frac{1}{\sqrt{CL}}, \quad (2)$$

which has a meaning of the natural frequency of oscillations of the arc current in the tuned circuit.

In addition, transform equation (1) into the following form:

$$I_a'' + \frac{\omega^2 L}{R} I_a' + \omega^2 I_a = \frac{\omega^2}{R} E - \frac{\omega^2}{R} U_a - \frac{U_a'}{L}. \quad (3)$$

There are two independent parameters of the power circuit in the model, i.e. ω and L. Their selection determines also the value of capacitance C according to (2).

Consider variations in current i and voltage u with respect to their stationary values I_{a0} and U_{a0}, for which we make the following replacement in equation (3):

$$I_a = I_{a0} + i; \quad U_a = U_{a0} + u.$$

Then, allowing for the relationship that determines the working point of the arc:

$$E = RI_{a0} + U_{a0},$$

transform equation (3) into the following form:

$$i'' + \frac{\omega^2 L}{R} i' + \omega^2 i = -\frac{\omega^2}{R} u - \frac{u'}{L}, \qquad (4)$$

thus deriving the linear inhomogeneous second-order differential equation that is the main equation of the mathematical model. It allows estimation of fluctuations of the current for the known dependence of fluctuations of the arc voltage upon the time.

Note that, when deriving equation (4), no assumptions were made on infinitesimal quantities of the values that enter into it.

Modelling of sequence of pulses in fluctuations of voltage. As known from the experimental results, an individual pulse of voltage formed due to shunting of the arc has a shape of a positive triangular pulse, the rise time of which is much longer than the decay time [1–4]. This shape is attributable to the fact that in the case of an approximately constant intensity of the electric field the arc voltage linearly grows with increase in the arc length. Assume that the ratio of the pulse rise to decay time is 9:1.

For the plasmatron with a channel diameter of 0.01 m and gas flow rate of 0.006 kg/s, at current $I = 110$ A and voltage $U = 410$ V the root-mean-square voltage of fluctuations is approximately 6 %, i.e. about 25 V [2]. Duration of one pulse is close to 1 ms. Shape of a pulse in fluctuations of voltage with the above parameters is shown in Figure 2.

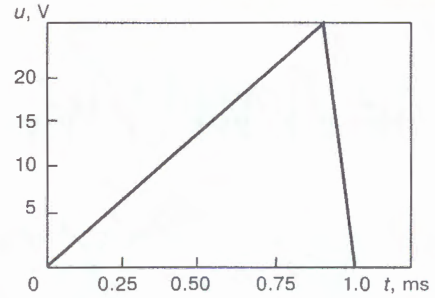

Figure 2. Shape of an individual pulse in fluctuations of voltage

Pulses in the fluctuations form a continuous random sequence, the amplitudes in which are distributed in accordance with the normal law relative to the mean value of the arc voltage [2].

Assume that breakdown between the arc and chamber walls that shunts the arc occurs each time at the same point. This means that the arc voltage after each jump returns back to its initial value. So, we will count off the voltage pulses from this value.

In this case the amplitudes of the pulses are distributed in accordance with the normal law with a mean value of voltage pulses $\bar{u} = 2\sigma$ and standard deviation σ.

This assumption does not substantially limit generality of the model, preserving a random character of the process, but leads to formation of a constant component of voltage pulses that is equal to

$$U_0 = \frac{1}{t} \int_0^t u(t)\mathrm{d}t.$$

To determine a variable component of voltage pulses, the zero level of sequence of the pulses should be increased by the above value.

Assume for the simplest variant of modelling of this sequence of pulses that the rate of rise of the pulses remains constant (it is determined by the rate of drift of the arc with the gas flow in the plasmatron channel), and that duration of the pulses is distributed in accordance with the normal law with mean value $\tau = 1 \cdot 10^{-3}$ s and standard deviation σ_τ. In this case the pulse amplitudes are also distributed in accordance with the normal law with a mean value of voltage pulses $\bar{u} = \sigma_\tau$ and standard deviation $\sigma_u = \alpha\sigma_\tau$, where α is the rate of the pulse rise.

Assume that the mean value of the pulse amplitude is equal to a double mean-root-square value of fluctuations of voltage, $\bar{u} = 50$ V. Then the rate of the pulse rise will be equal to

$$\alpha = \frac{\bar{u}}{0.9\tau}$$

and standard deviation of duration of the pulses will be equal to

$$\sigma_\tau = \frac{\sigma_u}{\alpha} = 0.9 \frac{\sigma_u}{\bar{u}} \tau = 0.45\tau.$$

Figure 3, *a* shows an example of the resulting variable component of a sequence of 20 pulses. Generation of sequence of random numbers distributed in accordance with the normal law, N (τ, 0.54τ), and determining duration of pulses in the sequence, as well as subsequent calculations were made in the Mathematica 4 system.

Calculation experiment. *Determination of fluctuations of the arc current*. Substitution of the determined sequence of pulses in fluctuations of voltage to the right part of equation (4) and its subsequent numerical solution allow derivation of the dependencies of the arc current fluctuations upon the time, similar to those measured in an actual experiment.

Figure 3, *b–d* shows calculations of oscillograms of the arc current fluctuations at different values of inductance L and product ωτ at $R = 1$ Ohm (the ωτ value equal to the ratio of the mean duration of a pulse in fluctuations, τ, to the inverse natural fre-

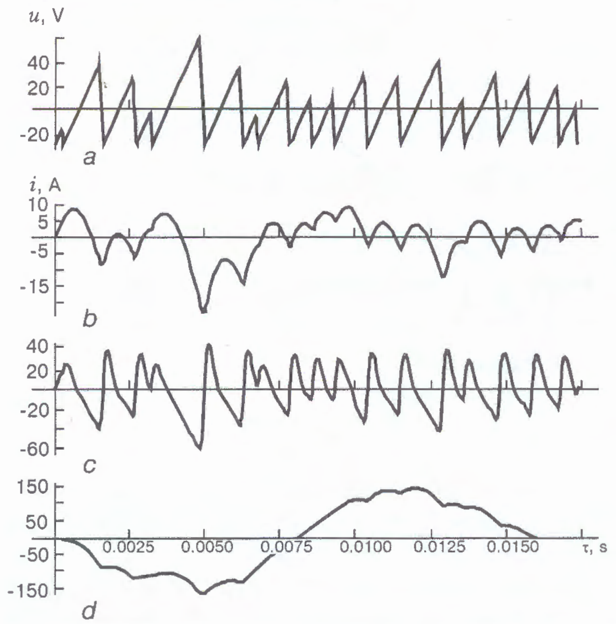

Figure 3. Variable component of a random sequence of pulses in fluctuations of voltage (a) and fluctuations of the arc current caused by it (b–d): b — $L = 1.0$ mH, $\omega\tau = 10.0$; c — $L = 0.1$ mH, $\omega\tau = 10.0$; d — $L = 0.5$ mH, $\omega\tau = 0.4$

quency of the system, $1/\omega$, is a characteristic scale of temporary processes in the power supply–arc system). This example shows dependence of the operating mode of this system upon the values of the circuit parameters. Values of fluctuations of the current increase with decrease in inductance and $\omega\tau$. In particular, variations of the current shown in the oscillogram (Figure 3, d) lead to extinction of the arc (current at the working point is 110 A). The mean-root-square value of the variable component of the current was selected to be the quantitative criterion of values of its fluctuations:

$$\Delta i = \sqrt{\frac{1}{t}\int_0^t i^2(t)dt},$$

and it is this mean-root-square value that is usually measured in the experiments.

The calculation experiment was conducted to determine dependence of Δi upon the system parameters. Dependence of standard deviation of the arc current upon $\omega\tau$ at different values of inductance of the circuit was measured during this experiment. Inductance was varied from 0.1 to 1.0 mH, which corresponds to the range of its values in power circuits of the plasmatrons designed for powder processing and metal cutting [2]. Duration of the sequence of pulses in the fluctuations was equal to 30 pulses. Each point was determined as a mean value by the results of 20 independent measurements with different random sequences of pulses in the fluctuations of voltage. The standard deviation of sampling was about 10–20 % of its mean value.

The curves in Figure 4 were plotted from approximation of the experimental points by a linear combination of the exponential and linear functions. The range of variations in $\omega\tau$ for each curve is limited from below by a condition of stability of the system with respect to small disturbances:

$$L = RCR^* > 0,$$

where R^* is the differential resistance of the arc [2]. By determining the value of ω, we obtain the condition for $\omega\tau$:

$$\omega\tau \geq \frac{\tau}{L}\sqrt{RR^*}.$$

Typical values of $R = 1.0$ Ohm and $R^* = 0.8$ Ohm were used for the calculations.

Results and discussion. As seen from the data shown in Figure 4, the dependence of Δi upon $\omega\tau$ is of the same character in all the cases, i.e. the standard deviation of the current decreases with increase in the $\omega\tau$ value and comes up approximately to a constant level at a fixed value of inductance.

The system will be in the oscillation mode if the following condition is met:

$$\omega\tau \leq 2\tau\frac{R}{L}.$$

In the case of $L = 0.10$, 0.25, 0.50 and 1.00 mH, this yields maximum values of $\omega\tau$ equal to 20, 8, 4 and 2, respectively. As follows from Figure 4, the values of Δi decrease with growth of $\omega\tau$ in the oscillation mode of the circuit and reach their maximum in the aperiodic mode.

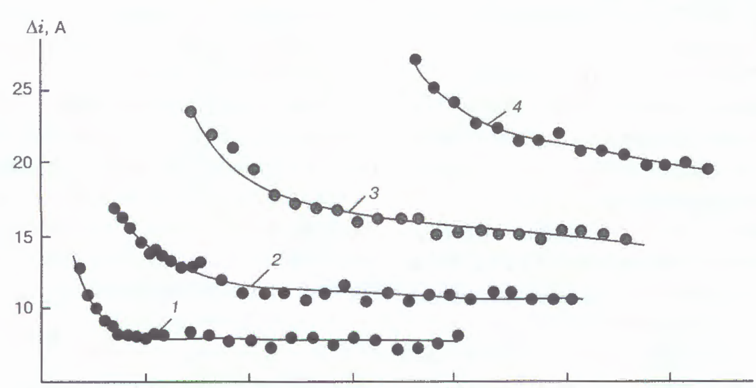

Figure 4. Dependence of standard deviation of current, Δi, upon $\omega\tau$ for different values of inductance of the circuit derived from the results of the calculation experiment: *1* — $L = 1.00$ mH; *2* — 0.50 mH; *3* — 0.25 mH; *4* — 0.10 mH

Increase in the ω value leads to growth of damping factor $\omega^2 L/2R$, decrease in amplitude of an individual pulse in disturbance of the current and increase in its duration. The pulses that follow are superimposed on the preceding ones, which leads to increase in mean deviation of the current. In the aperiodic mode, these two factors are likely to compensate for each other, and standard deviation remains constant.

Increase in standard deviation with decrease in inductance of the power supply–arc system can be explained from the structure of the main equation of the model (4). Decrease in inductance leads to decrease in the damping factor. Therefore, the same values of the factor as before will be achieved at higher values of ω. In this case the right part of the equation will substantially grow (approximately in proportion to ω^2), and it is this factor that leads to increase in disturbance of the arc current.

CONCLUSIONS

1. Values of fluctuations of the arc current depend mainly upon the inductance of the power supply–arc system. Increase in inductance smoothes out fluctuations of the arc current. The lower bound of the inductance value in the above system is determined by induction elements of the arc ignition circuit. An additional increase in inductance involves difficulties, as this inevitably causes growth of active resistance of the circuit and violation of operating conditions of the arc ignition circuit.

2. To decrease fluctuations of the arc current at a fixed value of inductance, the values of capacitance should be sufficiently low for the dependence of standard deviation of the current, Δi, upon $\omega\tau$ to reach a flat region ($\omega\tau = \omega/\sqrt{LC}$).

3. The quantitative estimates of the effect of inductance on fluctuations of the current and the values of $\omega\tau$ required for estimation of capacitance can be obtained by using the curves shown in Figure 4.

1. Zhukov, M.F., Koroteev, A.S., Uryukov, B.A. (1975) *Applied dynamics of thermal plasma*. Novosibirsk: Nauka.
2. Dautov, G.Yu., Dzyuba, V.L., Karp, I.N. (1984) *Plasmatrons with stabilised electric arcs*. Kyiv: Naukova Dumka.
3. Zhukov, M.F., Devyatov, B.N., Novikov, O.Ya. et al. (1987) *Theory of thermal electric arc plasma*. Part 2. Nonstationary processes and radiation exchange in thermal plasma. Novosibirsk: Nauka.
4. (1973) *Stability of electric arc burning*. Novosibirsk: ITF AN SSSR.

SOME ASPECTS OF ELECTRON BEAM WELDING APPLICATION

B.E. PATON and **G.I. LESKOV**
E.O. Paton Electric Welding Institute, NASU, Kyiv, Ukraine

The paper presents the energy properties of the electron beams as heat sources in welding. Possibility of welding structures of steel with up to 150 mm wall thickness, of alloys of aluminium (up to 250 mm) and titanium (up to 200 mm) is demonstrated. Features of thermal cycles of the metal of welds and HAZ and welded joint deformations are pointed out. Equipment is recommended for shop sections, where EBW of various items is performed. The main technological operations are described, which provide the high quality of welds.

Keywords: *electron beam welding, physical fundamentals, structural material, weldability, welding technology, welded structures*

E.O. Paton Electric Welding Institute began developing the technology and equipment for EBW starting from 1958 [1]. Powerful highly stable blocks fitted with computerized systems of control, diagnostics and documenting of welding results have been developed during this period. In the electron beam units of the new generation with vacuum chambers of 80 m^3 volume linear guides with positioning accuracy of ± 0.1 mm are used in the modules of displacement of the welding guns. Scientific fundamentals of EBW are being continuously developed, and various welding technologies are being introduced into aerospace, power and mechanical engineering sectors. Some of the experience gained in this field is generalized in this paper.

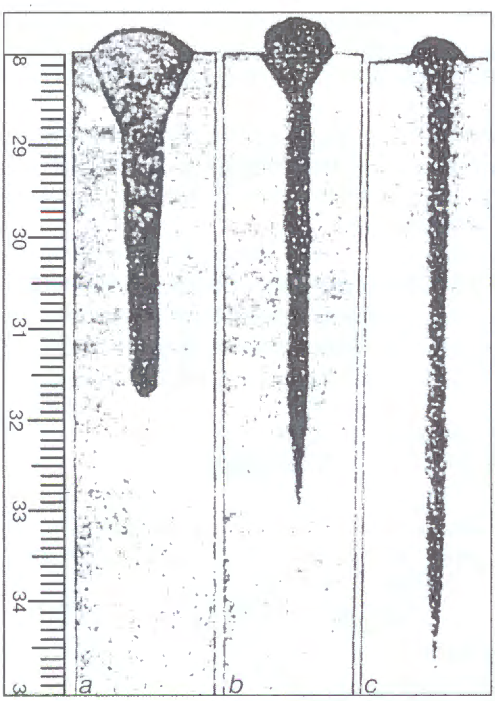

Figure 1. Macrosections of steel Kh18N9T welded by electron beams generated at different accelerating voltages: *a* — U_{acc} = 30; *b* — 60; *c* — 100 kV

It is known that at EBW power concentration ε in the heated spot is described by a normal-circular law [2]

$$\varepsilon = \varepsilon_0 \exp\left(-\frac{r^2}{r_b^2}\right),$$

where r_b is the effective radius of the beam, which is taken to be the distance from beam axis to the circumference line, where current density decreases ε = 2.718 times relative to the current density on beam axis.

Beam power concentration is maximum in the plane of the sharpest focusing, conditionally called the focal plane, and decreases with increase of the distance from this plane in keeping with the following ratio:

$$\varepsilon_0(h_1) = \frac{\varepsilon_0(h_0)}{K^2} = \frac{\varepsilon_{max}}{K^2},$$

where h_0 and h_1 correspond to the initial and current positions of the focal plane; $h_1 = Kh_0$; K is the coefficient of proportionality.

Currently used guns generate beams with the half-angle of convergence of about 0.02 rad. Penetrability of the gun at the same beam power, for instance 10 kW, changes significantly (Figure 1), depending on the value of accelerating voltage. With power increase up to 100 kW, steel penetration is equal to 150 mm, that of aluminium — 250 mm, that of titanium — 200 mm. Equipment developed at PWI operates at U_{acc} of 15 to 120 kW and has the power of 2 to 120 kW. Used lanthanum boride (LaB_6) cathodes in the form of washers of 4 mm diameter provide electron emission current of up to 1.2 A. The service life of such cathodes at admissible variation of beam parameters is from 10 to 40 h, depending on the operating conditions.

The heat source ensuring the through-thickness keyhole penetration should be analyzed as a concentrated source. Theoretically, the thermal efficiency of such a source η_t = 0.484 [3], which is confirmed experimentally [4]. Effective efficiency of the process of base metal heating by the electron beam η_s = 0.95, as the energy losses for radiation, including X-ray radiation, are minor. Full thermal efficiency of EBW should be calculated as

$$\eta_{pen} = \eta_s \eta_t = 0.45.$$

Volume of metal W, melted by such a source of power P, will be

$$W = HBv_w = \eta_t \frac{P\eta_s}{T_{melt} c\gamma},$$

where H and B are the average values of penetration depth and weld width, respectively; v_w is the welding speed; $c\gamma$ is the bulk heat capacity of the metal.

The penetration depth can be approximately estimated, using the following expression:

$$H = 0.4\eta_{pen} \frac{P}{v_w SB}, \qquad (1)$$

where S is the heat content of a unit of volume of molten metal (for low-carbon steel $S = 10.4$ kJ/cm^3). In the case of welding steels at $v_w = 2.5$ mm/s, $P/H = 0.20–0.25$ kW/mm, and this value is the reference point for the welding technologist, when selecting the modes of welding specific items. The modes are defined more precisely in welding test witness-samples.

In EBW with a sharply-focused beam the heat input

$$\frac{P}{v_w} = \frac{2HSd_b}{\eta_{pen}}$$

is 5–10 times less than in electric arc welding. P/v_w values, characteristic of EBW, should be incorporated into calculations of the thermal cycle of base metal, and evaluations of weld and HAZ structure. As is known from [3], cooling rate in single-pass welding of plates with initial temperature T_0 is equal to

$$\omega = 2\pi S \frac{(T - T_0)^3}{(P/v_w)^2}.$$

In EBW it is 25 to 100 times higher than the cooling rate in electric arc welding. In thermokinetic diagrams of austenite decomposition, as a rule, the curves of base metal cooling in EBW run to the left of the start of its decomposition and formation of hardening structures. Therefore, investigation of weldability of metals in EBW and modes of their heat treatment is the first mandatory stage of technological preparation in manufacturing.

The fastest method of evaluation of cold cracking susceptibility of metals to be welded is recording of acoustic emission signals, arising in welding and after it. Acoustic emission signals are recorded by special transducers, processed and converted into audible signals. They may be recorded on tape and registered by a counter as cracks [5]. Hot cracking susceptibility, not causing any acoustic emission, is evaluated on ring samples. EBW welds also develop specific defects [6], not found in electric arc welding, namely voids in the weld root («cold locks»), extended cavities in the cast metal (false channels) and narrow crevices in the plane of symmetry of the weld. Causes for and mechanisms of their development have been clarified in [6, 7]. Application of an oscillating beam is the most radical method of elimination of these defects [8]. Amplitude, frequency and modes of oscillation are selected experimentally, depending on the thickness of metals being welded.

Oscillating beams expand the root part of the penetration channels, and it is filled by liquid metal without «cold lock» formation. Beam axes move continuously over the front wall of the channels, thus eliminating undesirable depression of the pool in front of the middle of this wall. Inducing continuous oscillations of the pool, the beams promote filling of shrinkage cavities in the plane of symmetry of the welds.

Up to 30 % of all the publications on EBW are devoted to investigation of weldability of various metals by this process [9]. However, when developing the technology of EBW of specific items, the information in the publications should be regarded just as guidelines. Experience demonstrated the dependence of steel weldability on the method of steel production.

Let us consider the most significant results of investigations of weldability of some classes of steels, as well as aluminium and titanium alloys.

A great number of austenitic steels and alloys and high-temperature steels are currently widely used in different engineering sectors. Many of them are known to have poor weldability in arc welding. It is often impossible to avoid hot and cold cracks, or lower the probability of brittle fracture in the welds, etc. On the other hand, EBW is used extensively in fabrication of critical structures of dispersion-hardening alloy EP-202, martensitic steel of EP-609 class and high-strength steel 40KhNMA.

Aluminium-base alloys are welded without formation of cold or hot cracks or specific defects observed in welding of steels [10]. Properties of as-heat-treated welded joints are close to those of the base metal.

In titanium welding the welds also form without noticeable defects of discontinuity type. However, fine round pores may appear along the fusion boundaries. It is impossible to detect these pores with the existing methods of nondestructive testing of welded joints, and in most of the cases they are allowed by the codes.

Geometrical dimensions of welded components, including thicknesses of parts to be welded, are usually specified in the drawings. In EBW application the need to remove the root defects beyond the load-carrying section of the welded joint is taken into account. Possibility of using backing is considered, which can be left or removed, as well as of flanges on one of the abutted parts. Thickness of backing or flanges should be not less than 10 % of that of the parts to be welded [11].

When blanks for high precision items are made, it is necessary to envisage allowances on the butts to be welded, which will compensate for the transverse shrinkage of welds, dependent on their width.

Measurements of transverse shrinkage of welds in EBW confirm the applicability of the following equation [12] for evaluation of their magnitude:

$$\Delta_{tr} = K \frac{a}{S} \frac{q}{v_w}, \tag{2}$$

where a is the temperature coefficient of linear expansion; q/v_w is the heat input.

As in EBW the heat input is 5–10 times smaller than in electric arc welding, Δ_{tr} values are also 5 to 6 times smaller than in argon-arc welding.

Results of measurement of Δ_{tr} in EBW of samples of 20Kh12VNMF steel depending on weld width B demonstrated that $\Delta_{tr} = 0.1B$. The same Δ_{tr} value was obtained in EBW of discs of gas turbine rotor of steel 20KhN3M2FA and titanium alloy VT8.

Before assembly for welding, the blanks of ferromagnetic materials are checked for magnetization. Microteslameters of the type of EMTs-2-15, F-4356 etc. are used for this purpose. If the magnetic field induction at the edges being welded or elements close to them is higher than $1\cdot10^{-4}$ T, then the blanks should be demagnetized. Magnetic induction in the zone of the electron beam impact, exceeding $1\cdot10^{-4}$ T, causes its deflection together with the penetration zone by several millimeters. The butt cannot be welded, particularly in its lower part. The greater the thickness of the ferromagnetic items being welded, the higher are the requirements to their demagnetizing.

Experience of industrial application confirmed the reliability of EBW equipment (guns and power sources) of ELA type [13]. Differential pumping of the cathode–anode zone of the electron beam guns is performed by turbomolecular pumps. This eliminates electric breakdowns in the guns even at higher pressure in welding chambers (up to 0.55 Pa).

Power sources of the guns incorporate a powerful controlling pentode PP-2, providing stabilization of accelerating voltage and preventing development of breakdowns in the guns.

Selection of the focusing lens current requires particular attention, as the position of the electron beam focus relative to the surface of items being welded depends on the current value under the actual conditions of welding. Deep penetration and small width of the weld are achieved at focus location at half of blank thickness. A system of beam diagnostics has been recently developed [1, 14], which allows setting the beam focus in a specified point with the accuracy of ± 1 mm. To enable its functioning an area is allocated in the vacuum chamber for placing a massive target and a sensor in the form of a tungsten plate. Diagnostics is performed by «plate edge» method. Electron beam is deflected most of the time to the target and only 3 times per second in the opposite direction — to the sensor. Current flows in the circuit of the sensor, connected to the earth through a resistor. Computer analysis is applied to determine power distribution in the beam section and its effective radius.

Beam is oscillated by current running in the deflecting windings of the guns. Current oscillation amplitude is not more than 2 times greater than the keyhole diameter. Frequency (from 100 to 1000 Hz) is selected experimentally on samples. Its variation in a broad range only slightly influences the technological effect. The mode of oscillations has a much more significant influence. Longitudinal saw-tooth oscillations lead to greater depth of penetration and narrower welds [8]. Circular oscillations cause an inverse effect, but they are favourable for weld root formation, which is necessary for closing the circumferential welds.

In order to eliminate blank distortions under the impact of their own weight, it is rational to position large-sized shells vertically in welding. Stability of horizontal pools rises with narrowing of the welds:

$$\rho g B^2 = 2\sigma, \tag{3}$$

where ρ is the density of weld pool metal; g is the gravity.

It follows from (3) that in steel with $\sigma = 1.84$ J/m^2 the pool is stable in welding with an oscillating beam, if $B \leq 7.4$ mm and with edge beveling. Cross-sectional area of the removed metal in the groove should be equal to 8–10 % of anticipated weld cross-sectional area. This eliminates flowing out of 10 % of the metal beyond the welded edges, which occurs at its expansion in the pool.

A horizontal pool is particularly stable in welding of aluminium alloys due to low values of density of pool metal ρ and small weld width B. Up to 250 mm long welds without defects were made experimentally. Face and back beads in such welds are smoothed out with a lower power defocused beam of up to 5–8 mm diameter.

Optimum conditions of tack welding are strictly followed, namely mode, number, sequence required to minimize butt joint deformations.

Assembly-welding fixtures have an important role, as EBW produces narrow welds. It is important to satisfy certain conditions of blank basing during their machining for welding, as well as their fastening in an assembly jig. In a number of cases [11] finish treatment of the blanks is performed in the assembly-welding device.

Preliminary positioning of the assembly-welding fixture with the item in the chamber is performed by the operator manually or using a self-propelled carriage before pumping-down the chamber and switching on the electron beam. The alignment process can be followed using fiber-optic systems. Extremely high accuracy is achieved when using the beam proper to determine its actual position relative to the edges being welded. This principle is used in «Pritsel» and «Rastr» instruments, developed at PWI. The error of alignment of the beam with the butt should not exceed 0.2 mm, which should be controlled along the entire

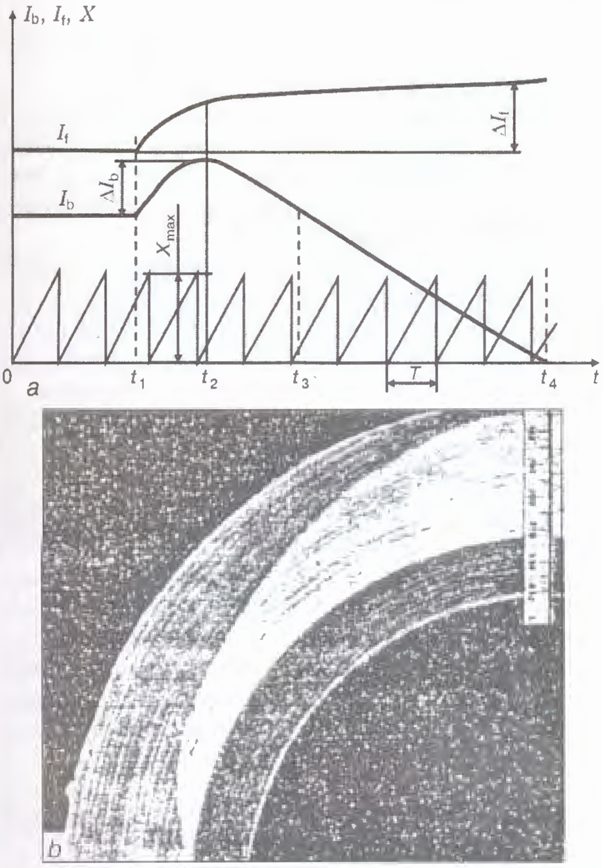

Figure 2. Nature of variation of the main parameters of the welding mode (a) and macrosection of the circumferential weld closure region (b)

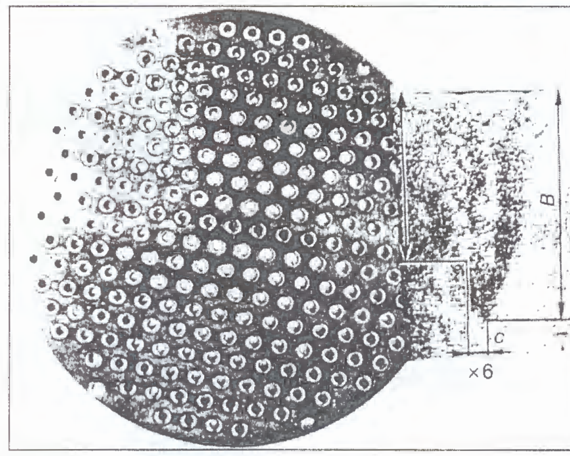

Figure 3. Butt joints of tubes and tubesheets made by EBW

length of circumferential and longitudinal butt joints. When a misalignment is observed, which exceeds 0.2 mm, it is necessary to find errors made during fastening of samples in the welding fixture, and examine the quality of the fixture proper and conditions of sample machining.

«Rastr» system of automatic following of the butt is applied in the case of welding complex-shaped butt joints [15].

In welding circumferential welds, it is necessary to ensure their closure without defects in the root part. This is achieved by increasing the diameter of the weld root. In order to avoid crater formation on the surface of weld closure section, its length should be not less than 4 to 6 times the maximum penetration depth of the weld.

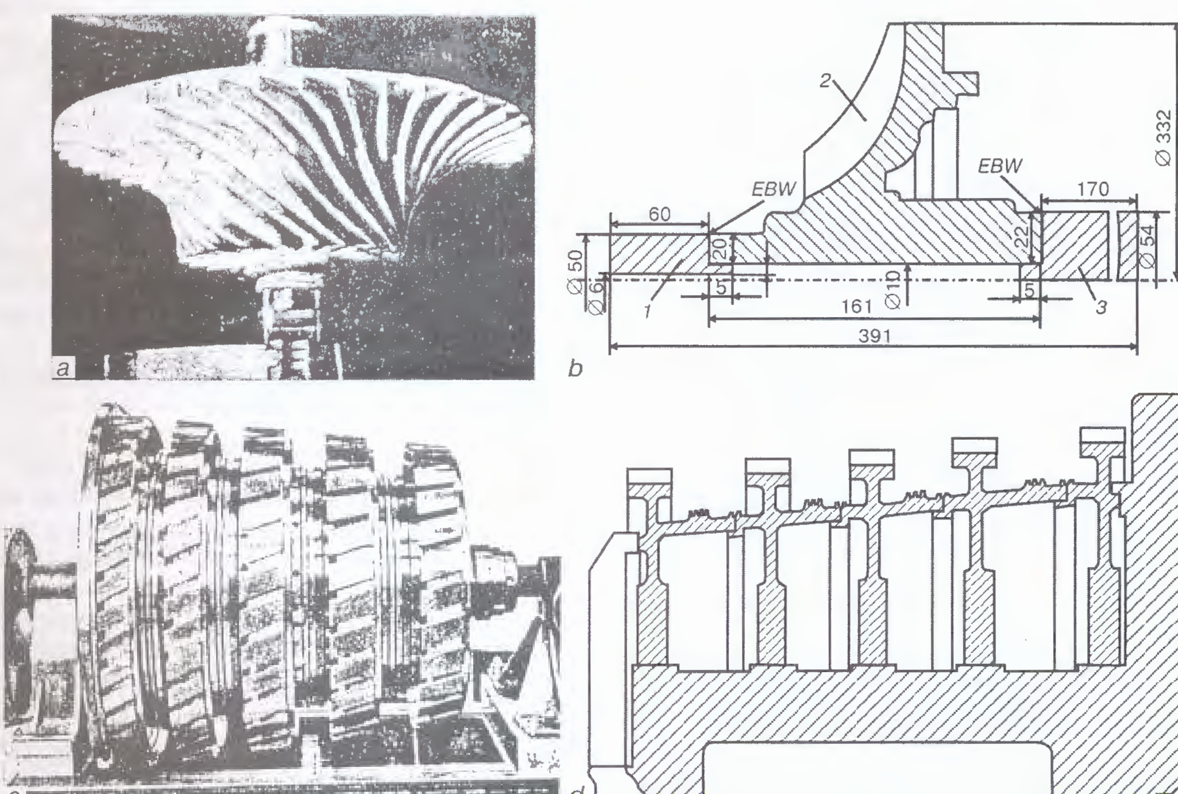

Figure 4. Cases of rotors of a gas turbine of alloy VZhL-14N (a) and compressor of alloy VT8 (c) welded by EBW, and their longitudinal sections respectively (b, d)

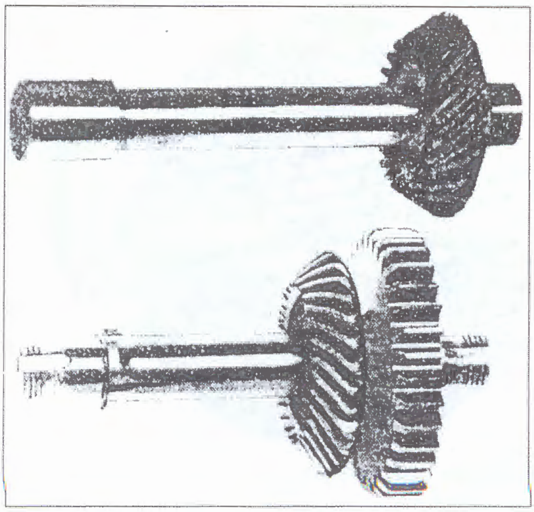

Figure 5. Gears of steel 18Kh2NMA for ship power units welded by EBW

The nature of variation of the main welding parameters at closure of a 40 mm deep weld on 12Kh1MF steel and macrosection of the closure section are shown in Figure 2. Defects in the weld root are eliminated by defocusing the beam through increasing beam focusing current I_f by 5 %. In order to maintain the penetration depth at the start of the closure portion, beam current is increased by 10–20 %, and then it drops to zero by a linear law. Amplitude of beam oscillations by a saw-tooth law is X = 2.5 mm, frequency being f = 500–600 Hz.

After welding test samples are subjected to heat treatment by standard or specially developed modes. Visual, X-ray and ultrasonic flaw detection in welded joints is performed. In the absence of defects, samples are cut out of the joints for strength, hardness, impact toughness, fatigue testing and metallographic examination by the standard procedures. Positive results of testing are indicative of the applicability of the selected technology for welding the actual standard items.

We will now give brief information about some of the effective industrial applications of electron beam welding.

EBW of tubes to tubesheets allows meeting the high requirements to strength and fatigue life of heat exchangers. In UL-178 unit developed at PWI in welding tubes of 8 and 11 mm diameter with wall thickness of 1.2 and 1.5 mm the depth of tube fusion with the tubesheets is 2.5 to 3 times greater than the wall thickness [16]. Circular scanning of the beam with f = 600–800 Hz and X = 0.2–0.3 mm was applied, in order to increase the stability of penetration depth and eliminate root defects.

A system of numerical program control, issuing commands to the servo drive, is used for displacement of the gun (or item) from one tube to be welded to another. Time parameters of welding are also assigned, i.e. the cyclogram of circumferential butt welding, including its closure, is followed. If required, the processes of alignment and welding can be observed on the picture monitor screen. Investigation of the mechanical properties of welded joints on tubes of austenitic, heat-resistant pearlitic steels and titanium alloys demonstrated their higher quality, compared to argon-arc welding (Figure 3).

In the Krasnoyarsk Engineering Plant, Russia, a significant improvement of the tactical and technological characteristics of the products has been achieved in welding large-sized casing shell structures for aerospace applications [11].

EBW is widely used for fabrication of aircraft engines, integrated wing panels, propellers, etc., this significantly reducing the cost of the aircraft [17].

In power engineering the high precision and strength of welded joints simplifies fabrication of blanks for large-sized components and ensures EBW cost-effectiveness in manufacturing rotor cases and shafts of gas turbines and compressors (Figure 4). EBW is very effectively used for gear blocks and components of car transmissions, tractors and ship drives (Figure 5). Science-Production Complex «Zarya-Mashproekt» is working with success in the field of welding components of gas turbines and compressors, drives of ship mechanisms, etc. Such work can be performed very efficiently in «Turboatom» Production Association in Kharkiv, Ukraine.

1. Paton, B.E. (2001) Modern electron beam technologies of the E.O. Paton Electric Welding Institute of the NAS of Ukraine. *The Paton Welding J.*, **2**, 2–7.
2. Rykalin, N.N., Zuev, I.V., Uglov, A.A. (1978) *Principles of electron beam treatment of materials*. Moscow: Mashinostroenie.
3. Rykalin, N.N. (1951) *Calculations of thermal processes in welding*. Moscow: Mashinostroenie.
4. Olshansky, N.A., Smelyansky, M.Ya., Tkachyov, L.G. et al. (1974) Effective and thermal efficiency of electron beam welding of thick items. *Svarochn. Proizvodstvo*, **12**, 1–3.
5. Trunov, E.N., Leskov, G.I. (1977) Device for evaluation of electron beam welding process by acoustic emission. In: *Proc. of 5th All-Union Conf. on EBW*. Kyiv: Naukova Dumka.
6. Paton, B.E., Leskov, G.I., Zhivaga, L.I. (1976) Specific nature of weld formatiön in electron beam welding. *Avtomatich. Svarka*, **3**, 1–5.
7. Paton, B.E., Leskov, G.I., Nesterenkov, V.M. (1988) Dynamic models of penetration channels in electron beam welding. *Ibid.*, **1**, 1–6.
8. Akopiants, K.S., Nesterenkov, V.M., Nazarenko, O.K. (2002) Electron beam welding of steels up to 60 mm thick with longitudinal beam oscillations. *The Paton Welding J.*, **9**, 2–4.
9. Nazarenko, O.K., Kajdalov, A.A., Kovbasenko, S.N. et al. (1987) *Electron beam welding*. Kyiv: Naukova Dumka.
10. Bondarev, A.A., Lobanov, L.M., Pivtorak, V.A. (1975) Investigation of mechanical properties of structure and deformations of EBW joints of 01420 alloy. *Avtomatich. Svarka*, **9**, 14–17.
11. Gupalov, V.K., Uspensky, N.V., Ugryumov, V.G. et al. (2002) Development of electron beam welding in Krasnoyarsk Engineering Plant. *Tekhnol. Mashinostroeniya*, **4**, 20–22.
12. Vinokurov, V.A. (1968) *Welding strains and stresses*. Moscow: Mashinostroenie.
13. Lokshin, V.E., Zubchenko, Yu.V., Tregubov, M.N. et al. (1980) Electron beam welding unit ELA 60/60 of 60 kW power. *Avtomatich. Svarka*, **6**, 36–40.
14. Akopyants, K.S., Nazarenko, O.K., Gumovsky, V.V. et al. (2002) System of diagnostics of electron beam in installations for electron beam welding. *The Paton Welding J.*, **10**, 27–30.
15. Nazarenko, O.K., Gorbunov, V.I., Shapoval, V.I. (1985) Operating conditions of «Pritsel-4» system for joint tracking in electron beam welding. *Avtomatich. Svarka,* **8**, 65–67.
16. Leskov, G.I., Trunov, E.N., Samusev, N.F. (1988) Electron beam welding of tubes to tubesheets of heat exchangers of pearlitic heat-resistant steels. *Ibid.*, **7**, 63–65.
17. Shnejderman, Ya.A. (1972) State-of-the-art and tendencies of development of electron beam welding in foreign aircraft and space industries. *Ibid.*, **6**, 38–43.

FLASH-BUTT WELDING OF RAILS. EXPERIENCE OF APPLICATION AND PROSPECTS FOR IMPROVEMENT

S.I. KUCHUK-YATSENKO, V.G. KRIVENKO, A.V. BONDARUK and **A.V. DIDKOVSKY**
E.O. Paton Electric Welding Institute, NASU, Kyiv, Ukraine

The paper describes an efficient process of flash-butt welding of rails, namely pulsed flash-butt welding, which was developed at the E.O. Paton Electric Welding Institute. This process allowed reducing the flashing allowance and welding time, while improving its stability and quality.

Keywords: *flash butt welding of rails, continuous flashing, pulsed flashing, in-process control, prospects for improvement*

Flash-butt welding of rails has been used with success in the railway transport for many decades, as it provides the highest and most stable quality of the joints, compared to other processes (thermit, electric arc). Advanced technology and equipment, developed at the E.O. Paton Electric Welding Institute in 1960s for welding rails, allowed this highly efficient welding process to be used also in the field conditions. Mobile machine-welding machines K355A, stationary machines K190P, K190PK, batch-produced by the Kakhovka Plant of Electric Welding Equipment,Ukraine for several decades, are widely used in railways of the CIS countries. Several hundred such machines are operating in Europe, USA, Canada, Japan, Australia and China.

Over the last decade intensive reconstruction of the railways has been in progress all over the world, new continuous welded and high-speed trunk railways have been built, and transition to laying higher strength rails is being implemented. Requirements to the quality of welded rails are increased, and these requirements cannot be satisfied without improvement of welding technologies and equipment. In development of the technologies of welding the currently available rails it is necessary to be able to vary in a broad range the heating of metal in the welding zone and thus provide a high reproducibility of the specified heating modes.

Technologies of welding rails, used abroad and in some of the machines used in CIS countries are based on the process of welding with intermittent resistance preheating and subsequent short-term flashing. Welding of currently produced rails is characterized by a high energy content of the process, so that it requires equipment of 500 to 700 kV·A power. Here it is not possible to ensure a uniform and concentrated heating, required in welding of high-strength rails. This is due to the fact that at short circuits the contact resistance drops to a minimum, and the useful power generated in the contact is much lower than the overall consumed power. The energy indices in flash-butt welding (power, power factor, energy consumption) are largely determined by the ratio of the resistance in the contact R_c between the parts and the welding circuit impedance $Z_{sh.c}$. Parameter R_c is determined by the accepted welding technology (heating by resistance or flashing). Lowering $Z_{sh.c}$ allows increasing the energy parameters in both the cases, although the effectiveness of this measure can be different, depending on the accepted welding technology.

There exist several approaches to decreasing $Z_{sh.c}$. One of them is lowering the frequency of alternating current in the welding circuit [1], or using direct current [2], which allows lowering $Z_{sh.c}$ value chiefly due to its inductive component. Another area, that has been pursued for many years at PWI, is development of special designs of the welding circuit of flash-butt welding machines, use of built-in transformers and parallel loops [3]. PWI experience shows that such a solution allows significantly decreasing $Z_{sh.c}$, actually both of its components (ohmic and inductive).

Flash-butt welding machines with low-frequency converters of frequency and number of phases did not become widely used in welding of rails. This is due to the need of applying cumbersome transformers and unreliable operation of the components of electronic control systems.

In development of technologies of welding and machine-welding equipment of the new generation most of the foreign companies over the last decades have followed the path of using direct current. Systems of current rectification using six pair of power diodes became the most widely accepted (Figure 1). Here a uniform load of the three phases and a sufficiently stable DC voltage are provided, energy parameters of the heating process are improved, more uniform heating of the parts over the section is achieved. Therefore, it seems possible to increase the current in the welding circuit, reduce the welding cycle duration and increase the heating concentration at the same set power, by lowering $Z_{sh.c}$ impedance. However, the thermal efficiency when using direct

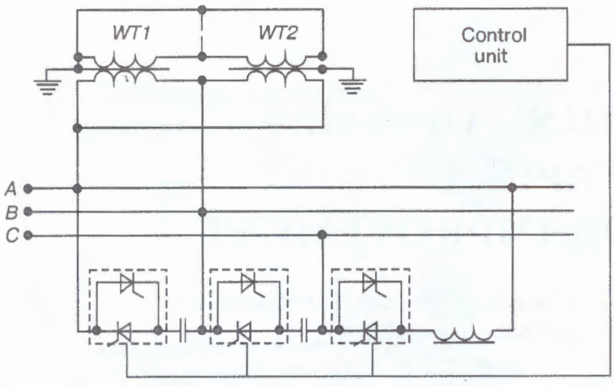

Figure 1. Schematic of rectification in the secondary circuit of the welding loop using six pairs of diodes (*WT1*, *WT2* — welding transformers)

current in this case is rather low, which is because of loss of a considerable part of the energy in the rectifier proper. At full load in the welding circuit the voltage drop in currently available diodes is 1.7–2.0 V, i.e. about 40 % of the total level of voltage drop in the secondary circuit of the welding loop of the machine. In addition, with resistance heating in the short-circuiting mode, the resistance in the contact between the parts remains low, as with alternating current, which predetermines the nature of heating, characterized by relatively low gradients of the temperature field in the HAZ (Figure 2, curve *1*). Transition to use of direct current does not provide a radical lowering of power in welding.

Power of the currently available machine-welding machines, operating at direct current, is equal to 460–600 kW, with the load being uniformly distributed for the three phases. Cooling water flow, when using the rectifiers, increases 3–4 times, compared to a single-phase machine of the same power, as the energy losses in the rectifier are greatly increased. In addition, when using continuous flashing, application of direct current turns out to be ineffective, as the resistance of the spark gap and the current change at

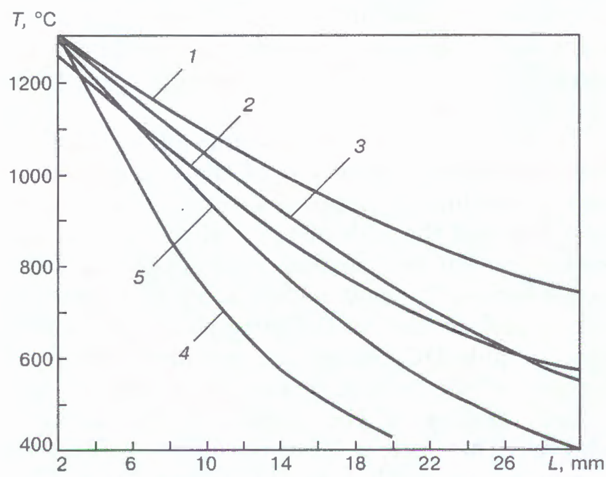

Figure 2. Temperature distribution in the HAZ metal before upsetting in welding R65 rails in different modes: *1* — with preheating (t_w = 200–250 s); *2* — continuous flashing with programmed voltage drop (t_w = 180–220 s); *3–5* — pulsed flashing at t_w = 110–120 s (*3*), 30–40 s (*4*), 70–80 s (*5*) (*T* — heating temperature; t_w — welding time; *L* — distance from flashing surface)

high frequency, thus increasing the inductance of the welding circuit.

Technologies and equipment, developed at PWI in the 1960s, are based on the process of continuous flash-butt welding without resistance heating [3]. At flashing the resistance in the contact between the parts is several times higher than at shot-circuiting, which significantly changes the part heating in welding. Most of the energy evolves in the contact between the parts, so that the losses in the secondary circuit are minimum. The power consumed in welding is 3 to 4 times lower than with resistance heating, respectively. Highly concentrated heating is ensured.

Continuous flash-butt welding is used extensively in various industrial sectors for joining thin-walled parts up to 20 mm thick. This process was not used for welding rails, as it did not provide the heating, required for joining thick-walled parts. Moreover, flashing of parts of large cross-sections did not seem to be possible without preheating. Methods and systems of regulation of the flashing process, developed at PWI, as well as new principles of designing the welding machines, allowed these problems to be solved and the technology of continuous flash-butt welding of rails with programmed regulation of the main parameters to be widely introduced. The technology is used with success both in the shop and field conditions.

It should be particularly emphasized that the welding technology is being improved continuously taking into account the new problems, raised by industry. One of such problems is development of the processes of intensifying the heating in order to improve the efficiency and optimize the heating conditions, required in welding the new categories of rail steel, produced by industry.

A method of pulsed flash-butt welding was developed [3], which is based on periodical short-time increase of the instant speed of flashing and of current up to values, close to $I_{sh.c}$, which is followed by its lowering to the specified level. Here the useful power, generated in the contact, increases briefly, and the overall value of current rises in flashing, as the process develops in time in *II* range (Figure 3). Higher current values at flashing are maintained on average. Effectiveness of such a process, as shown by experience of operating the first machines, is largely dependent on the characteristics of the used speed regulator and operating speed of the flashing drive. At insufficient operating speed the process of pulsed flashing cannot be maintained continuously, and the duration of pauses in current flowing is up to 40 % of the overall process duration, this lowering its thermal efficiency. In addition, at pulsed flashing the machine drive operates in the vibration mode, this shortening its life. Nonetheless, pulsed flashing allows 1.5 times reduction of welding duration and of flashing allowance, compared to continuous flashing or increased heating.

Technology of pulsed flash-butt welding has been so far used with success in operation of rail welding machines K355A-1 abroad. Technology of pulsed flash-butt welding is also used in joining complex-alloyed rails in stationary machines K190P, K190PK, when a higher energy input is required.

Investigations conducted at PWI over the last years resulted in development of new processes to increase the effectiveness of the continuous flash-butt welding process. Figure 3 gives the dependence of useful power evolved in the contact between the parts being welded, on electrical resistance of the load and current value in the welding circuit. The characteristic was taken in K190P machine in welding of rails in different modes.

Region *I* corresponds to the modes, accepted in continuous flash-butt welding of rails. Average power in flashing can be obtained from the power source at the established welding modes $U_{2o.-c} = 7.2$ V, $Z_{sh.c} = 95$ μOhm. In welding of rails in the modes, accepted in welding with intermittent resistance heating (region *III*), the useful power is below P_{max} value. Welding mode, corresponding to region *II*, provides the highest energy indices. It is established that at the consumed power close to extreme values P_{max}, the nature of flashing changes significantly. The process of explosion-like rupture of contracts is suppressed, duration of their heating in the solid phase is increased, and process of secondary melting prevails [4]. Such a process is unstable and cannot go on for a long time, changing to a regular flashing process (region *I*), or to short-circuiting (region *III*). The developed methods of regulation and systems of automatic control allowed producing a stable flashing process at extreme values P_{max}, irrespective of variation of the operating conditions (fluctuations of mains voltage, variation of welding circuit impedance and quality of dressing of the parts being welded). The new welding process was called pulsed flashing, it is patented in the leading countries [5], and implemented in welding of various parts, including rails.

Record of the main process parameters in rail welding by pulsed flashing in an upgraded K190P machine

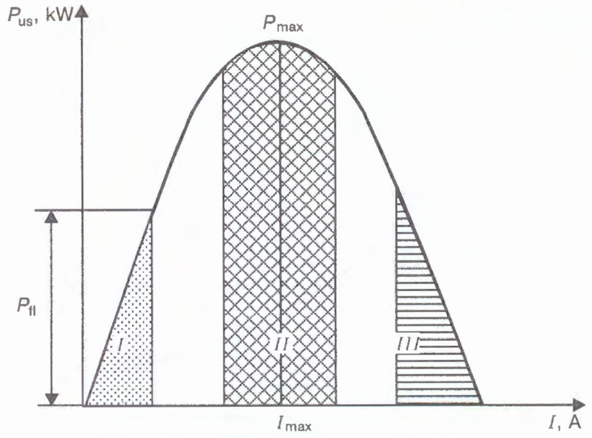

Figure 3. Dependence of useful power P_{us} on load resistance: *I* — welding current between the parts; I_{max} — welding current corresponding to the extreme power value P_{max}

is given in Figure 4. As is seen from the Figure, the current at pulsed flashing is 1.5–3 times higher than at continuous flashing, although the maximum values of current during flashing before upsetting and set power are the same in both the cases.

With pulsed flashing the duration of the process of welding and metal losses for flashing are reduced 2–2.5 times. The amount of gaseous evolutions in flashing, containing products of oxidation of iron, manganese and other alloying elements and impurities is reduced 10 times in rail steel, as the nature of flashing changes significantly. Melting of contacts without intensive vapour formation in the heated volumes prevails.

Use of pulsed flashing allows variation of heating in development of the technologies of welding rails of different composition. In addition to the possibility of applying the heating at low gradients of the temperature field (see Figure 2, curve *3*) providing the maximum energy input, in pulsed flashing a highly concentrated heating can be achieved (see Figure 2, curve *5*), which practically cannot be ensured with intermittent resistance heating or continuous flashing (see Figure 2, curves *1*, *2*).

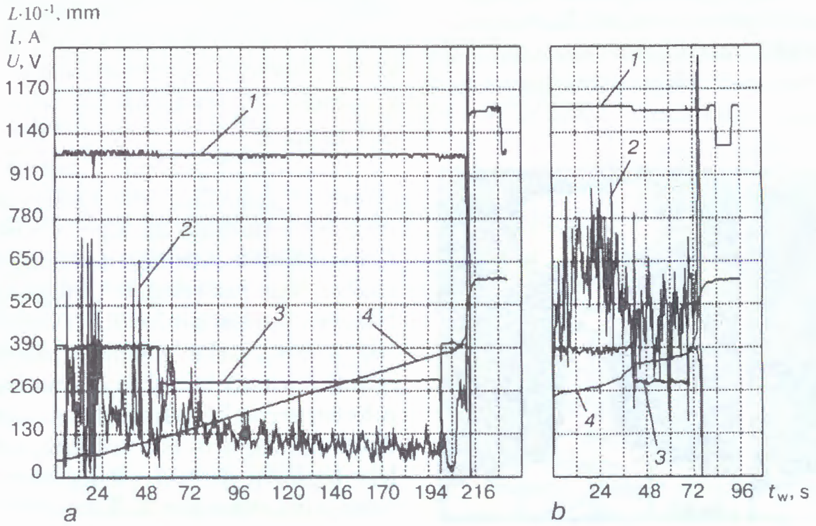

Figure 4. Record of the main parameters of welding R65 rails by continuous (*a*) and pulsed (*b*) flashing: *1* — pressure in the flashing and upsetting cylinders of welding machine; *2* — welding current; *3* — welding voltage; *4* — displacement

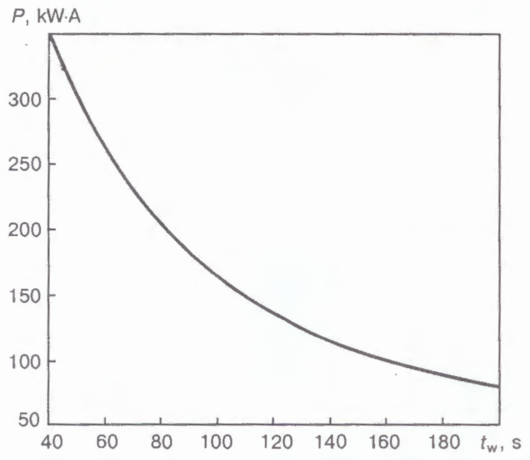

Figure 5. Dependence of consumed power P on welding process duration, plotted by the results of testing sound butts of R65 rails

At a high energy concentration in the contact between the parts, the near-contact metal layers up to 5 mm wide are heated up to the temperature (close to T_{melt}), required to form a sound joint at the minimum overall width of the HAZ and smaller softening of the metal in the welding zone.

Highly concentrated heating is applied at relatively low specific powers (25–30 VA/mm^2) uniformly over the entire cross-sectional area of the rail (R65 rails were welded, welding duration being 40 s). For comparison let us show that in welding in the established modes with intermittent heating of the same rails in a modern machine, fitted with rectifiers, specific powers were 80 VA/mm^2 (values are given for the secondary circuit of the welding transformer).

With pulsed flashing it appears to be possible to significantly reduce the set consumed power of the source by increasing the heating duration (Figure 5). Such a measure is fully justified in a number of cases in welding standard rails in the field.

Developed automatic systems of pulsed regulation allow maintaining a stable process at minimum open-circuit voltages ($U_{2o.-c}$ = 5 V) and set power of the source of 120–150 kW. Dependence of the consumed power on the duration of the welding process is given in Figure 5. At minimum powers the welding duration in equal to 70–90 s, HAZ heating does not exceed the values, used in welding with intermittent heating in the modern single-phase machines of 500 kW power.

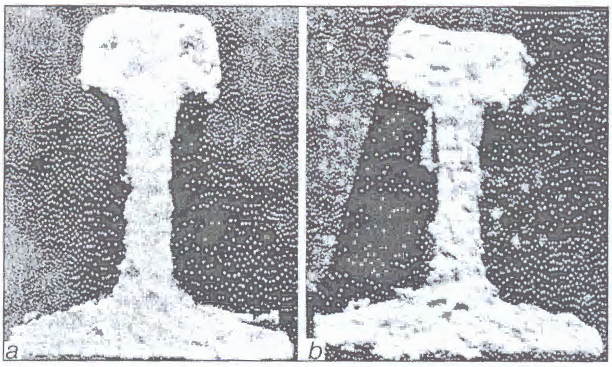

Figure 6. Flashing surface of R65 rails before upsetting in welding by pulsed (*a*) and continuous (*b*) flashing

In [3] it is shown that the quality of the joints in flash-butt welding is largely determined by the condition of the flashing surface of the parts being welded in the period preceding the upsetting. Defects found on the fracture surface of welded rails after testing, are most often due to formation of deep craters on the flashing surface, absence or thinning of the melt on the flashing surface.

At pulsed flashing the most even flashing surface is provided (Figure 6, *a*), and the melt thickness during flashing before upsetting is more stable than with canonical flashing (Figure 6, *b*).

Thus, favourable conditions are in place for complete removal during upsetting of oxide structures, formed on the flashing surface. Therefore, in pulsed flash-butt welding the probability of formation in the joint plane of defects of the type of dead spots or silicate inclusions is much lower than with other process of flash-butt welding of rails, which is particularly obvious in welding of complex-alloyed rails, which are currently produced.

In continuous and pulsed flash-butt welding the main parameters, determining the welding modes, are assigned by programs. Programmed variation of the parameters is performed in combination with use of feedbacks, which provide automatic correction of the set values of parameters at the change of the operating conditions. This ensures high reproducibility of the specified conditions of heating and deformation in welding in the case, if parameter deviations from the values set by the program do not exceed certain limits. Therefore, recording of such deviations during welding can be used for diagnostics of welded joint quality.

Many years of application of the technology of continuous flash-butt welding of rails, using the established methods of non-destructive testing, allowed accumulating a considerable bank of data, which demonstrates the interrelation between the joint quality and deviations of welding parameters from the specified values. Processing of these data, as well as simulation of different welding conditions with deviations from the established modes, resulted in determination of the criteria for evaluation of the quality of welding parameters by the recording instruments, using standard samples.

The control method, based on analysis of the diagrams of recording the main parameters, has been used over the last decade in welding of rails in the field in K900 machines operating abroad. In CIS such control was not used, although experience of its extensive application for flash-butt welding of pipes in the field is available. This is partly due to the absence of reliable multichannel instruments, required for parameter recording. In addition, interpretation of such diagrams requires the welding operators and controllers to have certain skills, and does not eliminate subjective assessments. Therefore, a computerized system of evaluation of welded joint quality has been used over the last years. It is based on algorithms, Comparative values of welding parameters for machine-welding machines of different types

Welding parameters	*K355A-1*	*K900*	*K920*	*K921*	*K922*	*K190PK*	*K1000*
Rated voltage of power source (mains), V	380	380	380	380	380	380	380
Voltage of diesel-electric set, V	400	400	400	400	400	–	–
Rated primary current (50 % duty cycle), A	395	395	540	540	540	395	800
Rated power (50 % duty cycle), kV·A	150	150	210	210	210	150	300
Rated working pressure in the hydraulic system, MPa	10	10	22	20	21	8.5	20
Rated upsetting force, kN (kgf)	450 (45000)	500 (50000)	1000 (100000)	1500 (150000)	1200 (120000)	500 (50000)	800 (80000)
Rated clamping force, kN (kgf)	1250 (125000)	1200 (120000)	2500 (250000)	3750 (375000)	2900 (290000)	100 (10000)	2000 (200000)
Weight, kg	2375	2600	3500	4200	3100	7000	8800
Overall dimensions, mm	810×1059×51140	1050×1300×1590	965×1300×1590	1090×1400×2430	1000×970×1895	2200×1060×3300	1170×2475×3620
Welding duration for R65 rails, s	180	180/90*	180/90*	180/90*	180/90*	180	180/70*

*For pulsed flashing.

developed as a result of statistical processing of experimental data.

Figure 7 shows the block diagram of a computerized system of welded joints control. It is based on PLC logic controller in combination with a computer. In such a configuration it allows controlling the welding process and fulfilling the functions of in-process control.

PLC program is developed so that the controller first analyzes the signals from the sensors, and based on their analysis a command is then issued for machine control. The control program algorithm allows tracing a number of possible unwelcome situations, leading to disturbance of stable flashing, and by acting on the flashing drive and power source eliminating these situations or interrupting their progress. In addition, the monitoring system also uses other sensors. Their signals are being continuously monitored. If any of the parameters goes beyond the tolerance range, the system reacts, depending on the importance of the parameter in the overall algorithm of quality assessment. Welding can be interrupted in the case of a gross violation of the process.

At individual deviations the signals are analyzed and all the obtained information is stored in the computer and simultaneously displayed in the digital (Figure 8, *a*) or analog (Figure 8, *b*) form.

After completion of welding the stored data are read and analyzed. In keeping with the incorporated quality algorithm, the system automatically takes a decision on this welded joint by the sound-reject principle. The result of analysis is displayed and automatically printed out so that by the end of the shift a general list is available of the butt welded joints with evaluation of their quality.

A special program has been developed for the computer, which allows a graphic presentation of the course of the welding process, as well as its individual stages on a larger scale. Information on each joint is

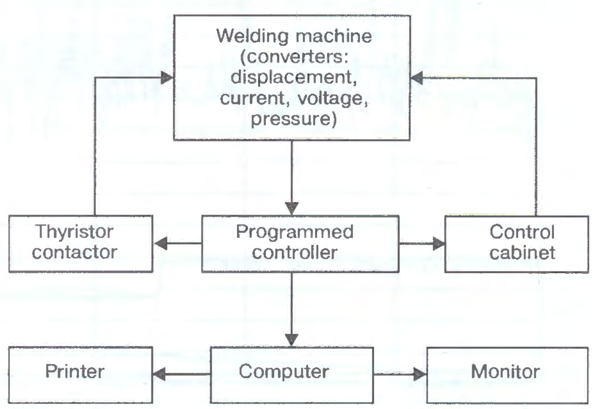

Figure 7. Block diagram of a computerized system of parameter quality control

Ukrzaliznytsa
South-Western Railway

PU-94 form
Appr. by UZ on 24.04.04. No.235-Ts

Kiev Machine-Welding Train
Machine-welding machine K1000 No.40

Shift Report

Foreman Evlov
Welder Kuzmenko
Flaw detection operator Skoretskaya

03.11.03

No.	Butt	Date	Time	Av. speed, v, mm/s	Allowance, S, mm	Time, t, s	Voltage, U1, V
			R65 — Continuous flashing				
1	Ref. 1	03.11.03	8:05:58	0.171	48.6	200	399
2	6	03.11.03	8:17:11	0.169	48.6	206	390
3	7	03.11.03	8:34:06	0.17	48.6	209	401
4	8	03.11.03	8:52:35	0.174	48.7	207	384
5	9	03.11.03	9:43:10	0.169	48.6	210	394
			R65 — Pulsed flashing				
6	Ref. 2	03.11.03	10:17:00	0.141	30.1	105	382
7	10	03.11.03	10:33:09	0.145	29.9	98	385
8	11	03.11.03	10:52:10	0.14	30.2	220	386

Cont.

No.	Voltage, U2, V	Current, I, A	Contr. of boost. speed, mm/s	Sh.-c. boost	Pressure, P, atm	Upsetting, P, mm	Upsetting with current, T1, s	In. upset speed, mm/s	$Z_{sh.-c}$, μOhms	Slipping	Result
					R65 — Continuous flashing						
1	302	180	1	No	99	12.3	1.5	45	84.9	No	Sound
2	302	183	1.1	No	99	12.2	1.4	54	86.7	No	
3	306	170	1	No	99	12.2	1.4	53	87.6	No	
4	302	164	1.1	No	98	12.3	1.4	60	87.6	No	
5	304	173	1.1	No	98	12.2	1.4	54	87.6	No	
					R65 — Pulsed flashing						
6	288	374	1.3	No	95	12.2	1.2	46	87.7	No	
7	292	377	1.2	No	96	12.2	1.2	48	87.9	No	
8	294	378	1.2	No	98	12.3	1.2	52	88	No	

Total: 8
Norm: 8
Reject: 0

a

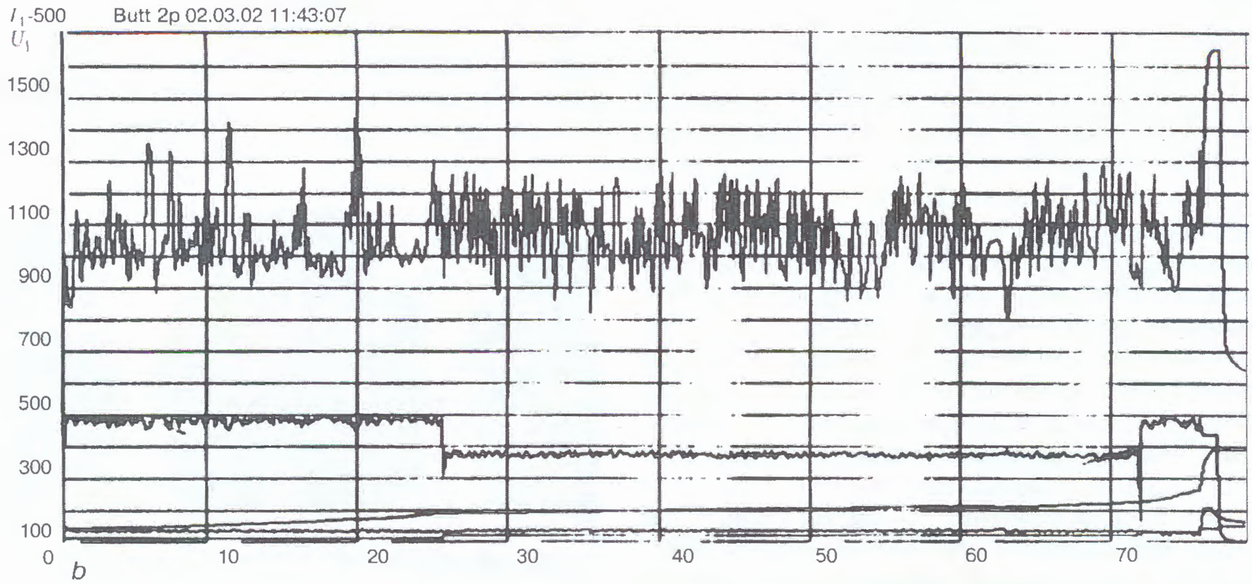

b

Figure 8. System of computerized control of the welding process: *a* — shift report; *b* — parameter recording

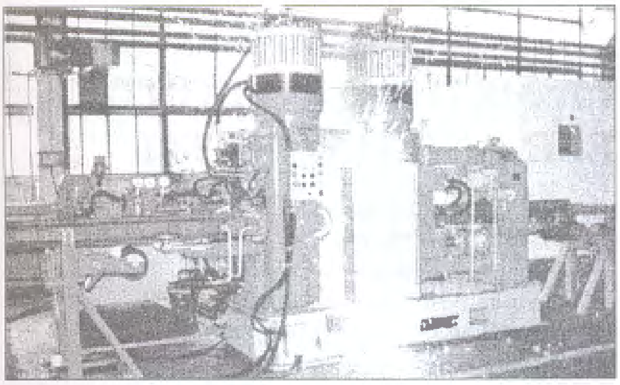

Figure 9. Machine-welding machine of K1000 type

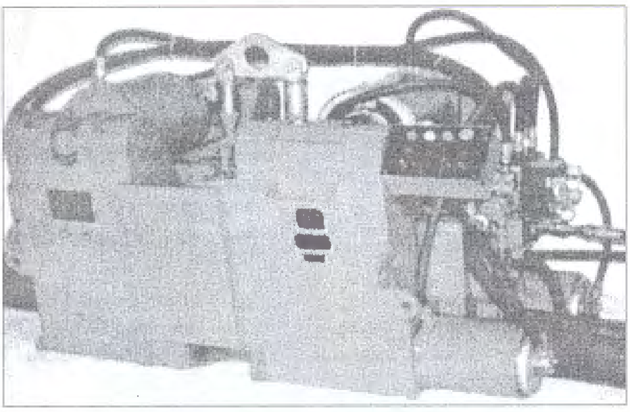

Figure 10. Machine-welding machine of K920 type

entered into the common data bank, accumulated during the welding machine operation.

The developed system of parameter monitoring can be implemented as a separate attachment, which is adapted to the currently operating machines K190P, K190PK, K355A of the previous generation. It consists of an industrial or home computer with a printer and electronics module, as well as a set of current, voltage, displacement and pressure sensors. In machine-welding machines of the new generation of K900, K920, K1000 type, it is a component of the overall system of control and monitoring.

Most of the machine-welding machine fleet available in the CIS before 1998 was made up by stationary machines of K190P, K190PK type and mobile machines of K355A-1 type, used in running machine-welding machine complexes. These machines, developed at PWI, were batch-produced by the Kakhovka Plant of Electric Welding Equipment for several decades. They use the technology of continuous flash-butt welding with program control of the main parameters. Experience gained over the many years of operation of this equipment is indicative of the highly stable quality of the welded joints.

Over the last 12 years PWI developed stationary and mobile machines of K900, K920, K1000 type of the new generation, batch production of which has been mastered by the Kakhovka Plant. Specification of this equipment is given in the Table. New machines are characterized by a higher efficiency, provide a higher accuracy of aligning, have built-in systems for flash removal in the hot condition. The machines feature a low short-circuiting resistance, are fitted with speed regulators and control systems, which allow automatic regulation of the main parameters of the welding modes. They incorporate a computerized control and diagnostic system of welded joint quality, which provides implementation of the technology of pulsed flash-butt welding.

This allowed development of up-to-date technology of welding high-strength rails. In pulsed flash-butt welding the values of their mechanical properties are higher than in welding with intermittent heating or continuous flashing.

The machine-welding enterprises of the Russian Federation are currently using 35 stationary machines of K1000 type of the new generation (Figure 9), made at Kakhovka Plant of Electric Welding Equipment. Starting from 2003 and in the next years introduction of mobile machines of K920 (Figure 10) and K922 type is planned. Their application will open up great possibilities in repair and reconstruction of continuously welded rail tracks. Increased forces of clamping and upsetting provided by the hydraulic drive of these machines allow welding long sections (up to 800 m), laid on the track, or performing welding with tension of the section being welded during repair of a continuously welded track.

1. Paton, B.E., Lebedev, V.K. (1969) *Electric equipment for resistance welding*. Moscow: Mashinostroenie.
2. Khazov, V.Ya. (1966) Electric processes in butt welding of aluminium and copper. *Avtomatich. Svarka*, **2**, 30–32.
3. Kuchuk-Yatsenko, S.I. (1992) *Flash-butt welding*. Kyiv: Naukova Dumka.
4. Kuchuk-Yatsenko, S.I., Bogorsky, M.V. (1978) Pulse flashing as a means of heat intensification in flash-butt welding. *Avtomatich. Svarka*, **2**, 11–15.
5. Kuchuk-Yatsenko, S.I., Bogorsky, M.V. *Method of flash-butt welding*. Pat. 46820 Ukraine. Int. Cl. B 23 K 11/04. Publ. 17.06.02.

PORTIONED HEAT INPUT AS A METHOD TO CONTROL STRUCTURE OF THE WELD AND HAZ METAL

A.T. NAZARCHUK, V.V. SNISAR and **E.L. DEMCHENKO**
E.O. Paton Electric Welding Institute, NASU, Kyiv, Ukraine

Peculiarities of manual arc welding with a portioned weld formation are considered. Advantages of this method compared with continuous arc welding include widening of the capabilities of controlling the weld and HAZ metal structure and improvement of mechanical properties and technological strength of welded joints.

Keywords: *arc welding, covered electrodes, pulsed-arc welding, portioned weld formation, portioned heat input, pilot arc, structure, hardness*

Unlike other methods of pulsed-arc welding [5–8], in welding with a portioned heat input [1–4] the weld consists of discrete, sequentially solidifying portions of the weld metal [1, 2].

Despite numerous examples of application of manual arc welding with a pulsed heat input [8–10], further improvement of the technology of manual arc welding is still a topical problem.

The purpose of this study was to raise the efficiency of manual arc welding with covered electrodes through using a portioned heat input to metal by ensuring a gradual solidification of discrete portions of the weld metal.

To do this, it is required that during pauses between periodic pulses of the basic arc current the arc discharge be maintained at minimum possible currents (3–15 A). In addition, depending upon the welding conditions and duration of a pulse, duration of a pause should be sufficient for solidification of discrete portions of the weld metal.

Standard equipment was upgraded allowing for these requirements. Designs based on a multiloop configuration of the welding circuit [4] were employed to ensure a portioned weld formation. In the first case the arc burning during pulses and pauses was maintained by the same welding loop. In the second case the welding circuit was made of two independently controlled loops, one of which provided burning of a low-power pilot arc needed to maintain conductivity of the arc gap, while the other loop provided burning of the main arc of a required power [4]. In this case the portioned weld formation can be achieved by using no special attachment that normally sets duration of pauses, t_{pause}, and pulses, t_{pulse}. For this, the arc gap was increased to a certain length at interruption of the main arc with the pilot arc continuing to burn. This method is attractive for welding in different spatial positions, when burning of the main arc and weld formation can be stopped any moment, but the low-power pilot arc can provide a reliable further ignitions of the main arc.

Experimental part of the study was carried out using the TD-251 transformer upgraded in a proper way to perform arc welding at a direct current (main arc). In this case the open-circuit voltage was $U_{o.-c}$ = = 55 V and the maximum welding current was I_w = = 250 A. The pilot arc was supplied from a separate power source with an open-circuit voltage of up to 80 V, and an adjustable range of the pilot arc current was 5–25 A. Duration of pulses and pauses was varied from 1.2 to 2.5 s. At the first stage the welding was performed by using the UONI-13/45 electrodes in flat position and on fixed butt joints of pipes.

To widen technological capabilities of the process, the portioned weld formation in flat groove welding was combined with use of a step-back method by depositing two layers per pass [2]. An additional regulation of the thermal welding cycle was provided by increasing the welding current to a maximum possible value. When making welds with a portioned-discrete formation, this can be achieved through increasing the current in a pulse and, at the same time, decreasing the pulse duration [2, 3].

As proved in the course of the work, a decisive effect on the process of the portioned weld formation in manual arc welding with periodic solidification of discrete portions of metal is exerted by the welding current in a pulse, I_{pulse}, and pause duration t_{pause}. Pulse duration t_{pulse} also affects the time of solidification of discrete metal portions. However, this parameter cannot be considered the basic one. Its choice is determined not by solidification, but depends upon the required amount of molten metal consumed for formation of the weld consisting of discrete, sequentially solidifying metal portions.

Approximate data on the dependence of pause duration t_{pause} upon the welding current in a pulse, I_{pulse}, are given in Table 1.

The portioned weld formation in manual arc welding offers substantial advantages over the welds made by continuous welding, especially welding of quenched steels, as well as welding in positions other than the flat one.

One of such advantages is increased resistance of welded joints to hot and cold cracking. Increased resistance of weld metal to hot cracking, as shown in [2], is provided by refining of primary crystalline grains during solidification of the weld metal, change in a direction of the impact front of the crystalline grains at the centre of the weld metal, disorientation of these grains, and change in character of growth of the crystalline grains in the weld metal showing up in their intermittent growth from layer to layer both in height and along the weld. Increased resistance of the joints to cold cracking is achieved due to an additional control of the thermal and, eventually, thermal-deformation welding cycle (TDWC) provided by changes of the duration of pulses and pauses, t_{pulse} and t_{pause}, as well as due to increase of the welding current

Table 1. Approximate values of t_{pulse} and t_{pulse} depending upon the pulse current I_{pulse} to ensure a portioned weld formation in flat position

I_{pulse}, A	t_{pause}, s	t_{pulse}, s
50–65	0.5–0.8	2.0–2.5
80–115	1.0–1.6	1.8–2.3
135–165	1.5–2.2	1.6–2.2
170–215	2.2–2.5	1.2–1.5

Note. Pilot arc current $I_{p.a}$ = 10–15 A.

[2, 3]. These parameters exert a decisive effect on the character of formation of the welds, providing a portioned character of their formation and periodicity of solidification of discrete portions of deposited metal.

Influence of the main parameters of the portioned weld formation, such as pulse and pause duration, t_{pulse} and t_{pause}, on the thermal welding cycle is of an ambiguous character [2, 3]. Increase of t_{pulse} and t_{pause} to a certain limit first causes a decrease in the rate of metal cooling to low temperatures, and then can lead even to its increase compared with the achieved optimum. Moreover, whereas the time of metal dwelling at high temperatures decreases with an increase in t_{pause}, increase in t_{pulse} leads to its growth. According to the data of [3], the effect of t_{pause} and t_{pulse} on the thermal welding cycle can be considerably increased by raising a critical value of the welding current and changing the welding speed.

As indicated in [2], it is recommended to apply such a portioned heat input in fusion arc welding of quenched steels which would cause a required periodic occurrence of the processes of melting, solidification and structuring of the weld and HAZ metal. However, as a result of changes in the heat input parameters, achieving it in the HAZ involves certain difficulties caused by peculiarities of propagation of heat in metal. Therefore, to ensure an additional control of TDWC in manual arc welding, the portioned weld formation in the experiments was combined with use of a step-back method by depositing two layers per pass.

In this case, one should take into account that the portioned weld formation is a key parameter for selection of the length of a step in welding by the step-back method by depositing two layers per pass. According to the data of [3], to ensure an equal temperature of self-heating, the length of a weld region with a portioned heat input should be much smaller than with a continuous heat input.

To control the process of mass transfer of the electrode metal, the use was made of an extra, third loop [4] consisting of a capacitor bank, the controlled discharge of which through the arc gap was provided by using a special thyristor switch. This design allowed the controlled mass transfer of the electrode metal in welding using the UONI-13/15 electrodes with a diameter of 4 mm at a current of about 25–35 A. It is believed that this results from peculiarities of release of the electric energy stored in the field of capacitors, i.e. the transfer of metal is associated with variation of the dynamic characteristic of the welding circuit.

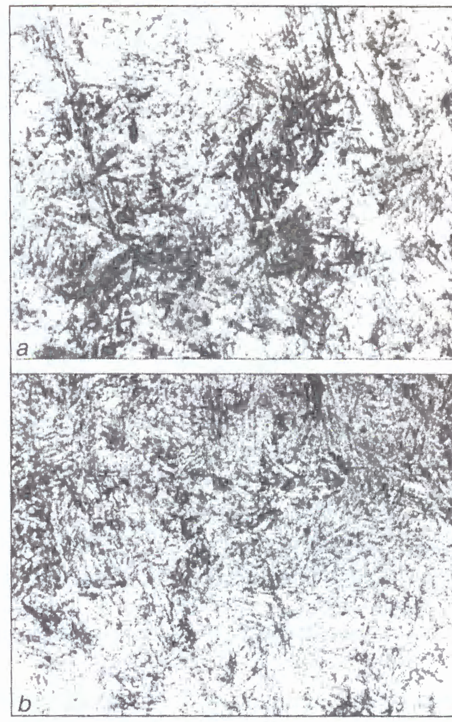

Figure 1. Microstructure of the austenitic-martensitic weld metal made by using electrodes ANVP-80 with continuous (*a*) and portioned (*b*) heat input (×400)

The three-loop configuration of the welding circuit provides operation in pauses of not only the loop that maintains conductivity of the arc gap (pilot arc), but also the loop that additionally controls mass transfer of the electrode metal. This configuration allows widening of the range of adjustment of the pause duration t_{pause}, which guarantees a reliable portioned weld formation with an intermediate solidification of discrete metal portions.

The portioned weld formation makes it possible to improve also mechanical properties of welded joints (Table 2) by changing to a certain degree the process of metal solidification and TDWC. In particular, it provides a marked improvement in ductile characteristics and impact toughness of the weld metal.

The use of the portioned weld formation seems highly promising for welding high-strength quenched steels without preheating and postweld heat treatment of welded joints, including by using new austenitic-martensitic consumables [11].

The first results were obtained in the course of study of the impact on structure of the austenitic-martensitic weld and HAZ metal in quenched steel by the portioned heat input.

High-strength steel 15Kh2N4MDA 40 mm thick was welded without preheating and postweld heat

Table 2. Mechanical properties of weld metal in welding of steel 09G2S using electrodes UONI-13/15

Weld formation	σ_t, MPa	σ_y, MPa	δ, %	ψ, %	KCU, J/cm², at T, °C	
					+20	−40
Continuous	460	360	26	65	220	180
Portioned	430–440	340–350	30–32	68	240–250	210–220

Note. Bend angle in both cases was 180°.

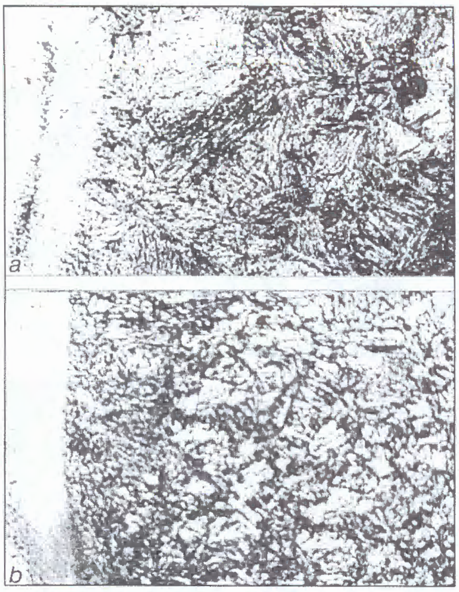

Figure 2. Microstructure of the HAZ metal in welded joints of quenched steel 15Kh2N4MDA made with continuous (*a*) and portioned (*b*) heat input (×320)

treatment by using experimental electrodes ANVP-80. Welding was performed with a continuous and periodic heat input. Test pieces were machined from the welded joints. Then microsections were made from the test pieces to examine structure of the weld and HAZ metal, and study distribution of microhardness in the fusion zone.

Metallography results show that a substantial refining of structure of the weld (Figure 1) and HAZ metal (Figure 2) was achieved in the case of a periodic heat input. The weld metal made by welding with a continuous heat input (Figure 1, *a*) is a mixture of stacked multialloyed low-carbon ($C \leq 0.03$ wt.%) substitutional martensite (*HV* 2700–3200 MPa) and retained austenite. The content of the latter is 8–12 wt.% at a continuous heat input and 10–14 wt.% at a portioned heat input. Moreover, retained austenite in the second case is distributed more uniformly (Figure 1, *b*), which has a strong effect on consistency of mechanical properties. In both cases martensite of the weld metal has a form of stacks of rectangular plates located along the boundaries of prior austenite grains. Thickness of the plates in a stack varies from 0.3 to 2.3 mm. Crystalline grains have an irregular shape. A central band, i.e. midrib, which is a concentration of twins, can be seen in the largest of the above grains. Characteristic feature of the rest of the crystalline grains, especially of the weld metal made with a portioned heat input, is a dislocation structure.

Structure of the HAZ metal is a mixture of bainite and tempered martensite (Figure 2). Bainite is dominant in structure of the HAZ of a welded joint in high-strength quenched steel 15Kh2N4MDA made with a periodic heat input, which is evidenced by a lower level of microhardness (Figure 3). This structure provides a higher resistance of the joint to brittle fracture (Figure 2, *b*).

Studies of the effect of the portioned heat input on redox processes occurring in the weld pool also present an interest. However, this issue requires further investigations.

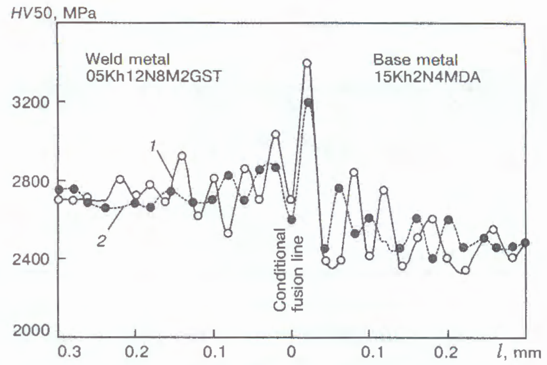

Figure 3. Distribution of microhardness *HV*50 in the zone of fusion of the austenitic-martensitic weld metal and steel 15Kh2N4MDA in welding without preheating and postweld heat treatment at continuous (*1*) and portioned (*2*) heat input (*l* — distance from a conditional fusion line)

It is not impossible that the combination of the low-amperage arc with an increased open-circuit voltage and the main arc with a decreased open-circuit voltage can also be used for plasma-arc cutting. It is believed that this will allow a reduction in weight and dimensions of the cutting equipment, and will enable (if necessary) the existing welding equipment to be employed to fit up the appropriate units.

CONCLUSIONS

1. Application of a portioned heat input with an alternating solidification of discrete portions of the weld metal for manual arc welding was proved to allow, e.g. in welding of quenched steels, an additional control of structure of the weld and HAZ metal, improvement in mechanical properties and widening of the capabilities of controlling the process in welding in different spatial positions.

2. It is shown that practicability of the process of welding with a portioned heat input can be raised through using a multiloop configuration of the welding circuit, where each loop performs its function by providing conductivity of the arc gap, portioned heat input and improved mass transfer of the electrode metal.

1. Nazarchuk, A.T., Lipodaev, V.N. *Arc welding method*. USSR author's cert. 1818180. Int. Cl. B 23 K 9/16. Publ. 30.05.93.
2. Nazarchuk, A.T. (1994) Control of weld metal solidification and thermal-deformation cycle in automatic arc welding. *Avtomatich. Svarka*, **5/6**, 3–9.
3. Nazarchuk, A.T. (1997) Influence of portioned-discrete weld formation on thermal cycle in fusion arc welding, *Ibid*., **5**, 13–17.
4. Nazarchuk, A.T. (2000) Improvement of process of consumable electrode welding with an intermittent arc. *The Paton Welding J*., **7**, 28–30.
5. Petrov, A.V., Slavin, G.A. (1962) Automatic pulsed argon-arc welding of sheet steel. *Svarochn. Proizvodstvo*, **2**, 6–9.
6. Paton, B.E., Potapievsky, A.G., Podola, N.V. (1964) Pulsed-arc consumable electrode welding with programmed control of the process. *Avtomatich. Svarka*, **1**, 1–6.
7. Zaruba, I.I., Lebedev, V.K., Shejko, P.P. et al. (1968) Modulated current welding. *Ibid*., **11**, 35–40.
8. Dudko, D.A., Zatserkovny, S.A., Sidoruk, V.S. et al. (1987) Influence of parameters of manual arc welding with modulated current on a weld shape. *Ibid*., **8**, 19–22.
9. Dudko, D.A., Sidoruk, V.S., Zatserkovny, S.A. et al. (1989) Dependence of weld chemical composition upon parameters of manual arc welding with modulated current. *Ibid*., **2**, 27–29.
10. Dudko, D.A., Sidoruk, V.S., Zatserkovny, S.A. et al. (1991) Technology of manual covered-electrode welding with modulation of parameters. *Ibid*., **12**, 59–60.
11. Snisar, V.V., Demchenko, E.L., Ivanchenko, E.V. (2000) Challenging technologies for high-strength steel welding without preheating and heat treatment. *The Paton Welding J*., **11**, 37–40.

EFFECT OF SLIDING CONTACT IN CURRENT CONDUCTOR OF TORCH ON STABILITY OF ARC WELDING PROCESS

G.A. TSYBULKIN
E.O. Paton Electric Welding Institute, Kyiv, Ukraine

Sufficient conditions were obtained which guarantee the asymptotic stability of the consumable electrode arc welding process in case when the electric field intensity in arc column and resistance of a sliding contact in a current-carrying tip vary within some known boundaries.

Keywords: *arc welding, consumable electrode, sliding contact, stability of welding process*

In work [1] the sufficient conditions, guaranteeing the stability of the process of arc shielded-gas consumable-electrode welding at electric field fluctuations in arc column, were obtained using the direct method of Lyapunov and generalized inequalities of Silvester. It was assumed that all the rest parameters of the process are constant, however, some of them are changed noticeably with time. In particular in [2], the resistance of a sliding contact in the current-carrying torch tip is changed randomly within the wide ranges in the automatic welding. This change in contact resistance during welding in the presence of electric field fluctuations in arc column and varying length of the electrode stickout can have a significant effect on the stability of the process proceeding proper.

In this article, the conditions were obtained, which make allowances for the ranges of possible changes in resistances of a sliding contact and electrode stickout, the fulfillment of which guarantees the welding process stability. Judging from the available publications, these conditions have not been yet known.

Let us write firstly the condition of stability, obtained in [1], for the case of changing intensity of electric field E in the preset known boundaries $E_s = \sup E(t)$ and $E_i = \inf E(t)$, but at a constant total resistance R of current-carrying leads, electrode stickout and sliding contact in a current-carrying tip. It has a form

$$\sqrt{E_s} - \sqrt{E_i} < \frac{S_a - S_s + R}{\sqrt{ML}}, \qquad (1)$$

where S_a and S_s is the curvature of volt-ampere characteristics, respectively, of arc and welding current source at a rated value of current; L is the inductance of welding circuit; M is the curvature of characteristics of electrode melting at a rated value of welding current and preset stickout of the electrode.

Let us now consider a case when alongside the change in a generalized rigidity of the process $\beta(t, \lambda)$ the change in a generalized coefficient of damping $\alpha(t, \lambda)$, included into a differential equation, is occurred:

$$\ddot{\lambda} + \alpha(t, \lambda)\,\dot{\lambda} + \beta(t, \lambda)\,\lambda = 0, \qquad (2)$$

where

$$\beta(t, \lambda) = \frac{ME(t, \lambda)}{L}, \quad \alpha(t, \lambda) = \frac{S_a - S_s + R(t, \lambda)}{L}.$$

The equation (2) describes the transition process with respect to variable $\lambda = l - l_\infty$ characterizing the deviation of arc gap length l from its steady value l_∞ [3].

As the law of changing the parameter $\alpha(t, \lambda)$ was not determined, and only the boundaries of its change $a \le \alpha(t, \lambda) \le A$ are known, where

$$a = \frac{S_a - S_s + R}{L}, \quad A = \frac{S_a - S_s + R + \Delta R}{L},$$

it is interesting to determine an interval within which there is no loss in stability of the welding process at any law of changing $\alpha(t, \lambda)$:

$$A - a = \frac{\Delta R}{L}, \qquad (3)$$

where ΔR is the range of a possible change in a total resistance R.

To determine the mentioned interval, we shall use a sufficient condition of asymptotic stability of the process (2), shown in [1], which can be presented here in a convenient form

$$A - a \le 4\sqrt{b}, \qquad (4)$$

where $b = \frac{M}{L} E_t$.

Using expressions (3) and (4) it is possible to write

$$\Delta R \le 4\sqrt{MLE_i}. \qquad (5)$$

Thus, inequalities (1) and (5) are the sufficient conditions of stability of the consumable electrode arc welding process with an intensity of electric field

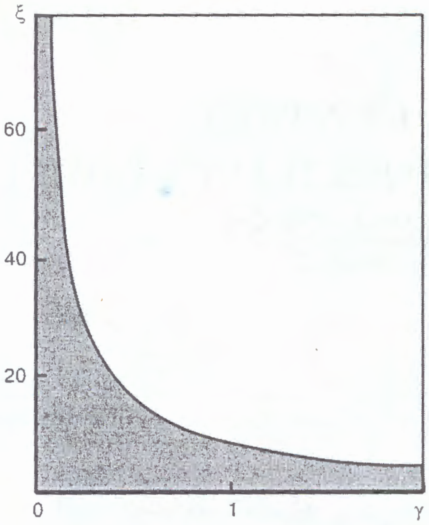

Figure 1. Region of stability of the arc welding process

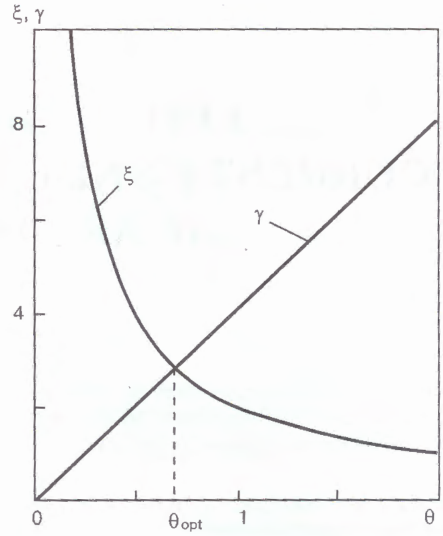

Figure 2. For determination of parameter θ_{opt} $\left(\xi = \frac{\mu + 1}{\theta};\ \gamma = 4\theta\right)$

in arc column and total resistance of a welding circuit, changed with time t.

For the further consideration, let us write the relations (1) and (5) in the form

$$\xi < \frac{\mu + 1}{\theta}, \quad \gamma \le 4\theta, \tag{6}$$

where ξ, μ, θ are the dimensionless parameters determined by formulae

$$\xi = \frac{\sqrt{E_s} - \sqrt{E_i}}{\sqrt{E_i}}, \quad \gamma = \frac{\Delta R}{R}, \quad \mu = \frac{S_a - S_s}{R}, \quad \theta = \frac{\sqrt{MLE_i}}{R}. \tag{7}$$

Hence, at $\xi \ne 0$ and $\gamma \ne 0$ it is possible to obtain the relation establishing the limitations for parameters ξ and γ:

$$\xi\gamma < 4(\mu + 1). \tag{8}$$

It is evident that at $\xi = 0$ and $\gamma = 0$ the sufficient condition of stability (8) is transformed directly into the required and sufficient condition $\mu + 1 > 0$, obtained earlier in work [3] for the case E, R = const.

Figure 1 shows the region of stability, determined by an equality (8). This region is limited by lines $\xi = 0$, $\gamma = 0$ and $\xi = 4\frac{\mu + 1}{\gamma}$. It follows from this Figure and expression (8), in particular, that the stability region depends greatly on μ. With its decrease, which can be caused by decrease in curvature of the volt-ampere characteristic of the welding current source S_s, the region of stability is narrowed.

By study of inequalities (1), (5) or (6), one more feature can be noted, associated with the presence of the inductance loop L in the welding circuit. It occurs that with its increase the range of changes in ΔR is widened, while the allowable interval for possible changes in intensity of electric field in arc column is narrowed. Consequently, there is an optimum value L_{opt}, at which both mentioned intervals have the maximum values. It is seen from inequalities (6) and Figure 2 that $\theta^2_{opt}(L) = \frac{\mu + 1}{4}$. Hence, with allowance for (7) we have

$$L_{opt} = \frac{R^2(\mu + 1)}{4ME_i}. \tag{9}$$

It is useful to use the relation (9) in the design of the technological equipment for the automatic arc welding.

CONCLUSIONS

1. To provide the stability of the consumable-electrode shielded-gas arc welding at continuously changed intensity of electric field and contact resistance at a current-carrying tip and resistance of electrode stickout, it is sufficient to fulfil conditions, formulated in the form of inequalities (1), (5) or (8).

2. With decrease in curvature of volt-ampere characteristic of the welding current source , the allowable intervals of fluctuations of electric field, contact resistance and resistance of electrode stickout are decreased. In addition, the optimum value of inductance in the welding circuit is also decreased.

1. Tsybulkin, G.A. (2002) About effect of electric field fluctuations in arc column on arc welding process stability. *The Paton Welding J.*, **6**, 38–39.
2. Hauck, G. (1989) Qualitaetsanforderungen an Drahtelektroden deim Schutzgasschweissen mit Robotern. In: *Roboter'89*.
3. Tsybulkin, G.A. (2002) To the question of GMAW stability. *The Paton Welding J.*, **5**, 14–16.

DEVICE FOR PROGRAMMABLE COMMUTATION OF WELDING CIRCUIT IN ARC WELDING EQUIPMENT

S.I. PRITULA, V.A. TKACHENKO, V.A. LEBEDEV and **Ya.Z. BURYAK**
E.O. Paton Electric Welding Institute, Kyiv, Ukraine

Capabilities of systems of commutation and adjustment, based on controllable transistor-type commutators, are systematized and described. The rationality of use of these devices is shown for the solution of a complex of technical and technological problems. Conception of modular designing of devices of a programmable commutation of the welding circuit using a controllable transistor-type commutator has been suggested.

Keywords: *arc welding, welding circuit, commutation, semi-automatic machine, cycle of operation, welding conditions, programming, modulation, synergetics*

Methods of arc mechanized welding and surfacing, as well as equipment for their realization (semi-automatic machines) are continuously updated. Recently, the designs of special transistor-type attachments for welding current sources have been appeared, which can solve a large complex of problems related to the control of electrode metal transfer, adjustment of welding conditions and so on [1]. The advanced element base makes it possible to design welding commutators, accessible for a wide circle of users. However, as far as we know, the appeared variants of designs of controllable transistor-type attachments, described in technical literature, have not been yet manufactured for mass application until now, at least in Ukraine.

The aim of the present work is to advertise a new design of a multifunctional controllable commutator of welding circuit, peculiar in its structure and design, for the specialists in the field of welding engineering. This development was realized using an accepted modular principle [2] to solve a wide range of problems of a different degree of complexity (Figure 1).

Let us consider the capabilities of a controllable transistor-type commutator shown in Figure 1. First of all, it is a simple commutation of the welding circuit, playing a role of a contactor in semi-automatic machines A-547Um, A-825M, which are manufactured by industry of Ukraine until now, that allows elimination of application of KM600, KM400 type contactors having a limiting service life, and also provides the functioning of the semi-automatic machine, which operates from the welding current source of any type.

It is the adjustment of the welding voltage level, realized at a high efficiency factor, that gives opportunity to solve the following problems:

• to provide a smooth change in voltage level from the welding current source of any type, within the required range;

• to use commutators also in manual arc welding, for example, instead of ballast rheostats in multi-station welding and also for organizing the stations of argon arc non-consumable electrode welding;

• to use commutators as basic built-in units in new designs of arc supply sources;

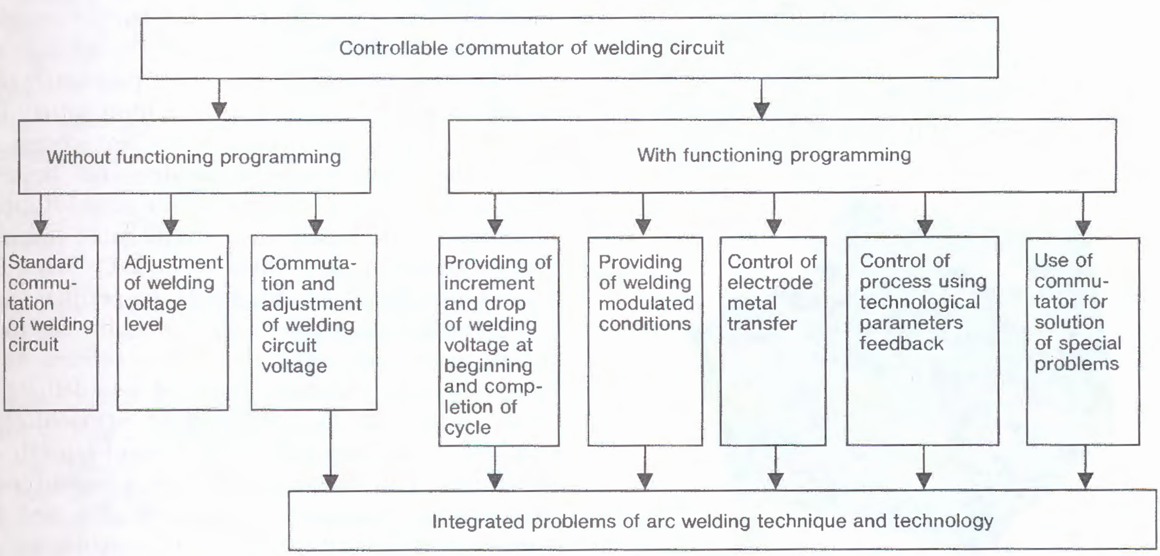

Figure 1. Capabilities of a controllable transistor-type commutator of welding circuit

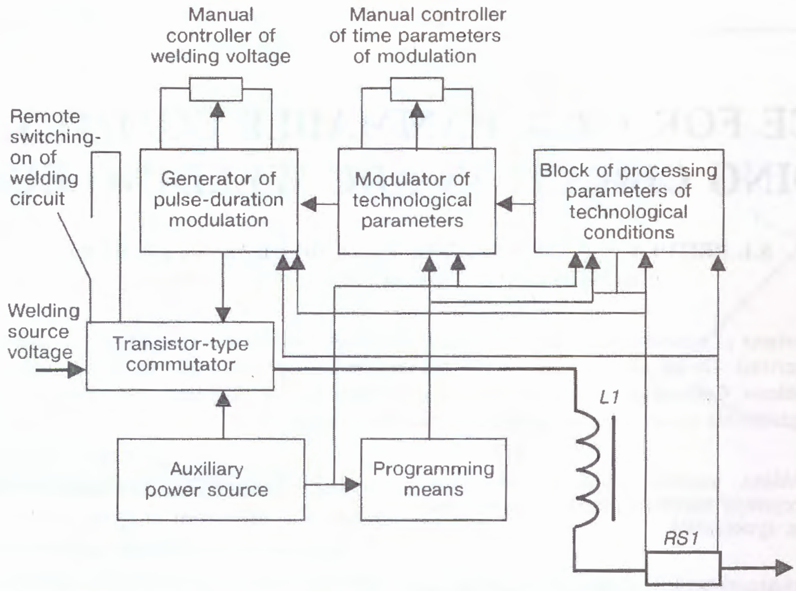

Figure 2. Schematic diagram of device of a programmable commutation of welding circuit based on a controllable transistor-type commutator (*L1* — choke; *RS1* — shunt)

• to use commutation as a basis for realization of technological innovations related to programming of arc mechanized process.

To form a controlling action, both an auxiliary power source and also a welding current source can be used. Adjustment of the welding voltage level is performed by a pulse-duration modulation of output voltage of a transistor switch, i.e. by change in a relative pulse duration, that is a positive factor for ordering the electrode metal transfer and welding process stabilizing.

Let us outline the capabilities of a controllable transistor-type commutator, which can be realized using relatively simple, but perfect enough means of control of operation of a transistor-type commutator, or as it is also called a chopper, using algorithms.

Among simple problems, there is a problem of programming the beginning and completion of the welding process with an appropriate increment and drop in voltage. However, sometimes, the process of arc exciting and quality of crater welding-up depend on the voltage level, and, in particular, in the period of stabilization and completion of the process. This refers, for example, to the arc mechanized welding of aluminium and its alloys, when unproper interval of time of the process completion can lead to the arc wandering at the current-carrying tip and coming-out of order of the latter. The same phenomenon can be observed also in equipment operation under the condition of riveting. In this case the quality of fulfillment of the technological operation is also deteriorated. In these and similar situations the application of programmable means of control of the transistor switch will be required. These means will be also necessary in providing the modulated condition of welding or surfacing when a synchronous operation of welding current source and electrode wire feed drive will be required to reach a full effect, and also in conductance of the technological process of welding or surfacing with a controllable electrode metal transfer realized using the welding current source. Developments in this direction [3] are mainly associated only with a change in a power condition of drop–weld pool system by changing the power parameters of the supply source by introducing the information about the technological parameters of the arc process.

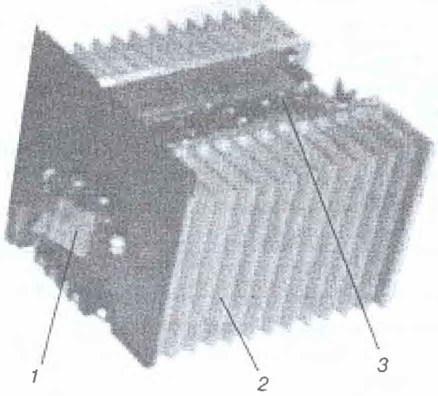

Figure 3. Transistor-type commutator: *1* — power terminal; *2* — radiator; *3* — transistors

All the above-described problems can be solved using a device of a programmable commutation of welding circuit, based on a controllable transistor-type commutator, developed at the E.O. Paton Electric Welding Institute (Figure 2). Its peculiar feature is the modular principle of designing, directed to producing system of separate blocks-modules, having those functions which are required by a definite customer, which can be combined into monoblocks or supplied to the customer in the form of separate subassemblies. The device is based on a transistor-type commutator, composed of parallel-connected field transistors with necessary means of matching and protection. The above-mentioned transistor-type commutator is shown in Figure 3. It can be used separately in the form of a contactless commutator of the welding

Parameters	*Relay KM-600D*	*Controllable commutator*
Dimensions, mm	120×120×10	220×350×160
Mass, kg	1.5	3.2
Number of operation cycles	$1\cdot10^3$	No limitations
Commutation current at 60 % duty cycle, A	600	500
Supply voltage of control circuits, V	27	Any required level
Price, $US	120	350

circuit. For this purpose the transistor-type commutator has contact and contactless inputs of control. When the transistor-type commutator is used in the form of a controller of arc voltage, a board of a pulse-duration modulation generator is added, having a modulation frequency of 10–72 kHz. In the configuration obtained, the problems of change in rigidity of external volt-ampere characteristics of welding current source, stabilizing of output parameter at oscillations of the input parameter can be solved. Owing to adding of one more board, i.e. a modulator of technological parameters, all the problems related to the problems of arc exciting, filling of crater, control of heat input into metal being welded are solved. The board can include current and voltage feedback signals. The modulator board of technological parameters can solve the problems of control of electrode metal transfer at the level of a pulsed effect of the transistor-type commutator on the molten metal drop at a definite (preset) moment of its formation at the consumable electrode end.

The device of the programmable commutation of welding circuit, based on a controllable transistor-type commutator, is designed in the form of a monoblock (Figure 4).

When necessary, the above block can be built-in into special recesses of welding current sources and also into those welding complexes where the semi-automatic machine with a described device is used as a local functioning unit. This block can be added with a system of the semi-automatic machine control, having a controllable electric drive, and also with separate units (*R–C*-circuits, formers of increment and drop of preset signal for a pulse-duration modulation generator), with the help of which the problems of arc exciting, crater filling, switching of welding conditions without arc interruption (manual modulation) are solved using simplified diagrams. The block can be built-in into a programming device. However, as the experience showed, it is better to install this device outside the block. In our developments, different designs of controllers with a comprehensive software were used as programming devices.

The above-mentioned developments were tested successfully in modification of the welding semi-automatic machine A825, which is completed with a transistor-type commutator, operating at the condition of

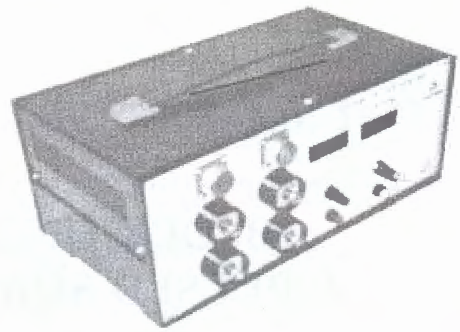

Figure 4. Device of a programmable commutation of welding circuit

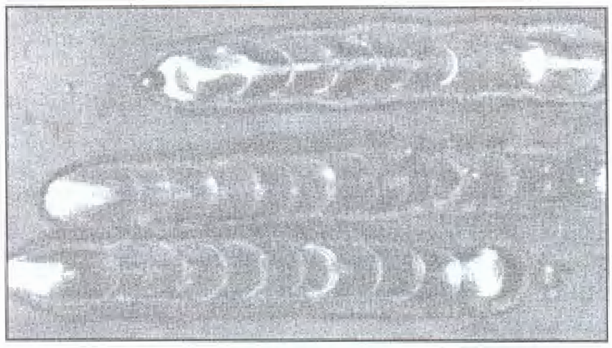

Figure 5. Samples of deposits made by the modified semi-automatic machine A825

voltage modulation and also in the semi-automatic machines of a modular design of PSh107V type. Figure 5 presents samples with deposits made by the modified semi-automatic machine A825 operating from the welding current source VS300B using 1.2 mm diameter electrode wire Sv-08G2s and modulation of conditions: $I_{a\,max} = 280$ A; $I_{a\,min} = 100$ A; $U_{a\,max} = 24$ V; $U_{a\,min} = 19$ V; $t_{pulse} = 0.6$ s; $t_{pause} = 0.4$ s (here $I_{a\,max}$, $I_{a\,min}$, $U_{a\,max}$, $U_{a\,min}$ – current and arc voltage, respectively, in a pulse and pause; t_{pulse}, t_{pause} – time of action, respectively, of pulse and pause). Figure shows deposited beads typical of a modulated process.

Technical characteristics of the transistor-type commutator and devices of a programmable commutation of welding circuit are given in the Table.

The suggested development can be used both as completing device for new designs of the arc mechanized equipment and also for modification of available semi-automatic machines of any types and purpose, including those with welding current sources, which have no smooth adjustment of the open-circuit voltage.

At present the device of a programmable commutation, based on a controllable transistor-type commutator, has been already prepared for a serial production.

1. Lebedev, A.V. (1992) Transistorised pulsed controller for mechanised arc welding. In: *New welding power sources*. Kyiv: PWI.
2. Lebedev, V.A., Moshkin, V.F., Pichak, V.G. (1998) Semi-automatic machines of standard modular design for welding, surfacing and cutting. *Svarochn. Proizvodstvo*, **1**, 24–28.
3. Saraev, Yu.N. (1988) Control of electrode metal transfer in short-circuiting arc CO_2 welding (Review). *Avtomatich. Svarka*, **12**, 16–23.